Chapter 11
Low-Cost Crop Waste Biosorbent Technology for Removing Toxics and Pollutants from Wastewater

Mayra Vera, Christian Cruzat, and María Eulalia Vanegas

Abstract Wastewater pollution is an urgent environmental concern. The negative effects of pollution on both humans and the environment have become a subject of intense discussion. Several techniques have been developed for the removal of pollutants from water. Most of these techniques adopt a combination of physical, chemical, and biological processes, which include photo-oxidation, chemical coagulation, sedimentation, filtration, disinfection, and adsorption. Nevertheless, adsorption is one of the most efficient methods for removal of pollutants from water, offering many economical, technological, and ecological advantages. The search for new low-cost technologies to remove contaminants from aqueous solution will be well embraced. Low-cost adsorbents can be employed to remove recalcitrant compounds from aqueous solution inexpensively and can be effective for removing both organic and inorganic contaminants. Biosorption technology using different biomasses (agro-industrial waste or organic waste that are considered composting material) is a promising alternative for the treatment of effluents that contain pharmaceuticals and heavy metals. These processes have certain advantages from both economic and environmental points of view, such as availability, abundance, the renewable nature of the adsorbent material, their low cost, and ease of operation of the treatment plant. Consequently, it is important to find low-cost alternative materials instead of traditional. Among the different agro-industrial wastes, sugarcane bagasse, cocoa shell, peanut husk, among others, are attractive materials for removing toxic heavy metals and pharmaceutical products from wastewater. To date, several researchers have reported on removal of different pollutants by using sorbents.

Keywords Wastewater · Water pollution · Biosorbent · Toxic removal · Agro-industrial waste uses · Biomasses

M. Vera (✉) · C. Cruzat · M. E. Vanegas
Centro de Estudios Ambientales, Departamento de Química Aplicada y Sistemas de Producción, Facultad de Ciencias Químicas, Universidad de Cuenca, Cuenca, Ecuador
e-mail: mayra.vera@ucuenca.edu.ec

P. A. Chong et al. (eds.), *Agricultural, Forestry and Bioindustry Biotechnology and Biodiscovery*, https://doi.org/10.1007/978-3-030-51358-0_11

Introduction

Contamination of the environment by heavy metals has become a major concern in recent years. Various industries produce and discharge wastewater containing heavy metals into the environment, posing a serious environmental threat to human health and the ecosystem. Untreated wastewater from industries and homes eventually end up in rivers and other aquatic systems that are a source of livelihood for humans. Most of these rivers are used as source of drinking water by rural dwellers without any form of treatment, thus increasing the chances of suffering ill health. Contamination and redistribution of toxic metals, metalloids, radionuclides in the environment as well as introduction of a plethora of organic pollutants necessitates ever-increasing standards of pollutant detection and treatment. The deleterious effects of organic and inorganic pollutants on ecosystems and on human health are well known, and huge expenditure is devoted to industrial treatment methods to prevent or limit discharges. Apart from physical and chemical methods of treatment, biological methods have been in place for many years such as standard sewage and water purification treatments as well as auxiliary reed bed and wetlands approaches.

Heavy metals are known to persist in the environment and become a risk for aquatic organisms. Biosorption uses the ability of dead/inactive biomass to remove heavy metals from aqueous solutions. The major advantages of the biosorption technology are its effectiveness in reducing the concentration of heavy metal ions to very low levels and the use of inexpensive biosorbent materials. The utilization of agro-wastes as adsorbent is currently receiving wide attention because of their abundant availability and low cost. In recent years, applying biotechnology in controlling and removing heavy metal pollution has received much attention, and gradually became a hot topic in the field of metal pollution control because of its potential application. An alternative process is (bio)sorption, which can be defined as the removal of metal or metalloid species, compounds, and particulates from solution by biological materials. The idea of using locally available, low-cost agricultural plant materials for the research make sorption the preferred method.

Biosorption

Biosorption can be defined as a physico-chemical process used for removing substances from solution by biological material through spontaneous redistribution; traditional definitions were generally related to removal of heavy metals by microbial material (Gadd 2008). However, due to recent research, new applications have extended the definition, and nowadays the term biosorption has been extended to remove other compounds, such as dyes, pharmaceutical products, drugs, fertilizers, and pesticides, using living or dead biomass including all kinds of microbial, plants, and derived products.

Biosorption process therefore involves a liquid phase (aqueous solution) containing the sorbate (inorganic or organic pollutants) and biosorbent (substrates of biological origin).

There are a lot of biological materials that have a high potential for removing pollutants under environmental applications, including living biomass (fungi, algae, other microbial cultures) (Kumar et al. 2016), industrial solid wastes (sewage sludge, activated sludge, fermentation) (Norton et al. 2004; Hammaini et al. 2003), agricultural solid waste (fibres, leaves, fruit peels, rice straw, sugarcane bagasse) (Ali et al. 2012; Nahar et al. 2018), and natural residues. However, the constant challenge is employing biomass that is cheap, abundant, renewable, efficient, and environment-friendly.

The cost and value (valorization) are the major principles of sustainable development in a strategy for using local available agriculturally based biosorbents. This overall concept evaluates the technical feasibility for biosorption processes that can give added value. Agricultural wastes have high percentages of cellulose, hemicellulose, and lignin that contain a variety of functional groups (amine, carbonyl, hydroxyl) responsible for adsorption. Many researchers used cheap biosorbents such as nut shells, fruit peels, bagasse waste, risk husk, corncobs, olive oil factory waste (Abdolali et al. 2014; Malkoc et al. 2006; Peñafiel et al. 2019b), among others. The modification with pretreatments can modify the surface, increasing binding sites (de Oliveira et al. 2019). Therefore, by-product or agro-industrial waste are promising materials for being readily available and low-cost biomaterials, and these materials can be disposed of without expensive regeneration, reducing total treatment cost.

Mechanism of Biosorption

Due to the high variety of functional groups, biosorption is a complex process affected by several mechanisms that can operate simultaneously. The activity of the functional group can appear as a possibility for ion exchange and for formation of a donor–acceptor complex, as well as the ability to form chelate poly-ligand spatial complexes (Nikiforova and Kozlov 2016). There are many factors affecting biosorption processes, such as chemical structure, molecular size, charge, and available surface area.

Physical adsorption is a surface phenomenon with no specific interaction, and can involve weak Van der Waal forces, hydrogen bonds, polarity and steric interactions, dipole-induced dipole interaction, $\pi - \pi$ or electrostatic interaction (Ali et al. 2012); therefore, it is a reversible process and dependent on pressure as well as temperature. The functional groups have non-selective affinity for the metal ion species and bind to a wide range of metals and have been evaluated as monocomponents; but in most cases, when there are more than one type of metal ion, the removal of one may be influenced by the presence of other (Sud et al. 2008). In a

multicomponent system, there exist a competition for the adsorption sites on the surface, although the metals have generally the same charge, and the smallest size ion has a best adsorption favourable with highest adsorption capacity. For example, when metal ions such as Cd(II) and Pb(II) are studied in a bimetal solution in batch mode using banana peel, the mobility of the lighter ion (CdII) is more than the heavier ion (PbII) and makes adsorption favourable (Muhamad et al. 2010; Anwar et al. 2010).

Ion-exchange, where the metal ions are binding by replacing the initially occupied charged ion on biosorbent, is a reversible mechanism. Witek-Krowiak and Reddy (2013) reported the removal of Cr(III) and Cu(II) from aqueous solutions using soya bean meal, and the biosorption mechanism was due to ion-exchange, chelation and further precipitation of metal ions on the surface of biomass.

Another mechanism is the precipitation of insoluble metal species as metal oxides and hydroxides on biomass surfaces. Many cases are reported where the sorption is enhanced with pH value, but that is not a real adsorption process improvement; it is an alternate sorption mechanism, where the bulk solubility limit is reached, and the metal ion is removed from aqueous solution by the bulk precipitation. A surface precipitation model includes an initial, rapid, adsorption mechanism followed by a slower surface precipitation covering the adsorbed layer (Schneider et al. 2001). Therefore, it is important to consider the metal ion speciation as a function of pH in order to evaluate the precipitation contribution in biosorption process.

Complexation involves a ligand centre in the biomass (atoms with lone pair electrons to donate) like divalent oxygen (hard acids), trivalent nitrogen atoms or sulphur atoms (soft acids), and can form monodentate or multidentate ligands for binding metal species. The concept of hard/soft ligands predicts the bonds formed, ionic or covalent respectively (Gadd 2008). This mechanism can inhibit desorption.

Chelation can be defined as a binding of a metal ion with an organic molecule (ligand) to form a ring structure. Amine groups play an important role in metal ion binding. The chelation takes place through dative bonds with the lone pair of electrons within nitrogen present in the $–NH_2$ groups of biomasses. Panda et al. (2007) reported that the binding of Ni(II) on husks of *Lathyrus sativus* was probably chelation through dative bond formation.

Finally, when other pollutants are present in synthetic and real aqueous solution (other metal ions and organic materials), metal biosorption capacity can change through synergism, antagonism and non-interaction. Calculating the adsorption rates can illustrate the effects in multicomponent conditions, and the presence of co-solutes could enhance the intermolecular forces between pollutants.

Parameters Affecting Biosorption

Different factors affect the biosorption rate which include temperature, pH value of solution, nature of biosorbents, surface area-to-volume ratio, concentration of biomass, initial metal ion concentration and metal affinity to biosorbent.

Under batch conditions, a biosorbent is mixed with a metal-containing solution within a simple reactor and operated until thermodynamic equilibrium is reached. In a continuous-flow system (packed bed), synthetic wastewater is continuously fed to a biosorbent column with an upward or downward stream.

Factors Influencing Batch Biosorption

Studies in adsorption by batch experiments (discontinuous) provide a measure of the efficiency of adsorption in removing specific elements and the maximum adsorption capacity. In addition, they are useful in determining optimum operating conditions (solution pH, particle size, contact time, solute concentration, temperature, agitation rate, etc.) as well as the mechanisms involved in the process. Of these, the pH usually plays a major role in biosorption and seems to affect the solution chemistry of metal ions or another pollutant (metal, dyes, pharmaceutical compounds) and the activity of the functional groups of the biomass.

Temperature For efficient removal of metal ions from environment samples, the optimum temperature needed to be investigated. It is generally assumed that biosorption is carried out between 20 and 35 °C. High temperatures above 45 °C may result in adsorbent damage which in turn affects metal uptake process (Abbas et al. 2014; White et al. 1997; Ahalya et al. 2003; Goyal et al. 2003). As temperature increases, it usually enhances biosorptive removal of adsorptive pollutants by increasing surface activity and kinetic energy of the adsorbate but may damage physical structure of biosorbent (Park et al. 2010).

pH The pH of the solution is the most important parameter which affects the surface charge of biosorbent, the degree of ionization, and speciation of the adsorbate – all of which affect the sorption of the sorbent material, solubility of metal ions and number of binding sites on the biomass. The kinetics of sorption strongly depends on the initial pH of the solution since at lower pH, the biosorption of metals is affected (Greene and Darnall 1990; Deng and Wang 2012). General range of pH for metal uptake is between 2.5 and 6. Above this limit, metal uptake ability of biosorbent gets compromised (Abbas et al. 2014).

It has been shown that the affinity of cationic species for the functional groups present on the cellular surface is strongly dependent on the pH of the solution. The biosorptive capacity may be low at low pH values, and increases with pH until reaching an optimum level. However, at higher pH (8 and upwards), metals begin to precipitate due to formation of M(OH). At low pH values, cell wall ligands are closely associated with hydronium ions and restrict the biosorption of M^{n+} as a result of competition between H_3O^+ and M^{n+} with bacterial biosorbent cell wall ligands. As the pH increases, more ligands, such as carboxyl, phosphate, imidazole, and amino groups, would be exposed and carry negative charges which attract M^{n+} and biosorb it onto the cell surface (Joo et al. 2010).

Effect of agitation speed As agitation speed increases, it enhances biosorptive removal rate of adsorptive pollutant by minimizing its mass transfer resistance, but may damage the physical structure of a biosorbent (Park et al. 2010).

Effect of biosorbent size If biosorbent size decreases, it is favourable for batch process due to higher surface area of the biosorbent, but not for column process due to its low mechanical strength and clogging of the column (Park et al. 2010).

Concentration of biomass The concentration of biomass is directly proportional to the metal uptake (Abbas et al. 2014; Gadd and White 1985; Modak and Natarajan 1995). Metal uptake depends on biding sites. More biomass concentration or more metal ions may restrict the access of metal ions to binding sites (Nuhoglu and Malkoc 2005). The dosage of a biosorbent strongly influences the extent of biosorption. In many instances, lower biosorbent dosages yield higher uptakes. An increase in the biomass concentration generally increase the amount of solute biosorbed, due to the increased surface area of the biosorbent, which in turn increases the number of binding sites. Conversely, the quantity of biosorbed solute per unit weight of biosorbent decrease with increasing biosorbent dosage, which may be due to the complex interaction of several factors. An important factor at high sorbent dosages is that the available solute is insufficient to completely cover the available exchangeable sites on the biosorbent, usually resulting in low solute uptake. Also, as suggested by the interference between binding sites due to increased biosorbent dosages cannot be overruled, as this will result in a low specific uptake (Bilal et al. 2018).

Initial metal ion concentration The initial concentration provides an important driving force to overcome all mass transfer resistance of metal between the aqueous and solid phases (Zouboulis et al. 1997). Increasing amount of metal adsorbed by the biomass can be dependent upon initial concentration of metals. Optimum percentage of metal removal can be taken at low initial metal concentration. Thus, at a given concentration of biomass, the metal uptake increases with increase in initial concentration (Abbas et al. 2014).

Effect of contact time It is necessary to identify the step that governs the removal rate of sorption process using different models kinetic.

Effect of initial concentration of sorbate In general, the isotherm studies for solid–liquid systems are carried out by changing the amount of sorbate in the solution. The performance of the sorbents is usually gauged by its uptake, which can be calculated by fitting the Langmuir isotherm model to the actual experimental data.

Taking account that biosorption is an eco-friendly and cheap method of removing metals from the environment, research conducted during last five decades has provided vast amounts of information about different types of biosorbents and their mechanism of metal uptake, with examples given in the following sections.

Fly ash was used as a low-cost sorbent for the removal of Cd(II), Pb(II), and Cr(VI) ions from aqueous solutions. The influence of pH, initial concentration of metal ions, equilibrium contact time, and temperature were studied using batch sorption experiments. The equilibrium for Cd(II), Pb(II), and Cr(VI) ions was attained with 90-, 100-, and 120-min contact times, respectively. The optimum pH values for Cd(II), Pb(II), and Cr(VI) removal were found to be 8.5, 6.5, and 2, respectively, with the sorption kinetics fitting a first-order kinetic model (Khan et al. 2009).

Dinesh and Kunwar (2002) investigated the use of low-cost activated carbon derived from bagasse, an agricultural waste material, as a replacement for the current expensive methods of removing heavy metals from wastewater. With a view to find a suitable application of the material, activated carbon has been derived, characterized and utilized for the removal of cadmium and zinc. The uptake of cadmium was found to be slightly greater than that of zinc and the sorption capacity increased with increase in temperature. The adsorption studies were carried out both in single- and multi-component systems. Studies were conducted to delineate the effect of temperature, initial adsorbate concentration, particle size of the adsorbent and solid-to-liquid ratio. It was concluded that the adsorption occurs through a film diffusion mechanism at low as well as at higher concentrations.

The biosorption characteristics of Cr^{6+} from aqueous solution using sugarcane bagasse was investigated. Experimental parameters affecting the biosorption process, such as pH, contact time, initial metal concentration, and temperature were studied. The Cr^{6+} biosorption onto sugarcane bagasse was favoured by pH, temperature 25 °C, and with 10 $g.L^{-1}$ biosorbent dosage (Alomá et al. 2013).

A biosorption experiment of the heavy metals (Fe, Cr, Cu, Mn, and Zn) was conducted without controlling for any experimental parameters (e.g., pH, temperature, or other compounds present in the effluent samples) by using four agricultural wastes or byproducts, namely rice husk, sawdust, lemon peel, and eggshell in which 20 g of each biosorbent was added to 1 L of effluent samples and stored for 7 days. The biosorption capacity of each biosorbent is ranked as follows: eggshell, sawdust, rice husk, and lemon peel. Furthermore, the biosorption affinity of each metal ion was found in the following order: Cu and Cr (both had similar biosorption affinity), Zn, Fe, and Mn (Nahar et al. 2018).

In this study, two agricultural residues, cotton stalks and apricot seeds, were used to adsorb copper and lead in solutions. Sorption capacities of agricultural wastes were significantly affected by solution pH, adsorbent mass and adsorbent particle size. The adsorption efficiency of two agricultural waste was in the order cotton stalk > apricot seed and the agricultural wastes adsorbed metal ions in the order of Pb > Cu. This study has indicated that cotton stalk and apricot seed could be employed as low-cost alternatives in wastewater treatment for the removal of heavy metals (Kahraman et al. 2008).

Pagnanelli et al. (2002) have carried out a preliminary study on the use of olive mill residues as heavy metal–sorbent material. The results revealed that copper was maximally adsorbed in the range of 5.0–13.5 $mg.g^{-1}$ under different operating conditions.

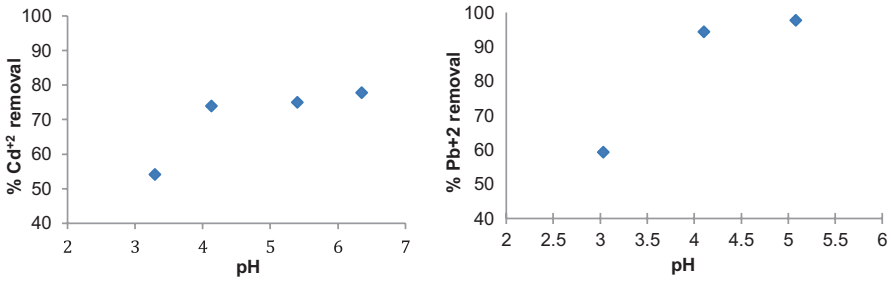

Fig. 11.1 Effect of pH on removal of cadmium and lead

Vera et al. (2016) investigated the use of sugarcane bagasse as a biosorbent in removing lead and cadmium from a mining wastewater sample. The parameters affecting the biosorption process, such as pH, contact time, concentration of the metal species and kinetic biosorption was studied. According to Fig. 11.1, best percent cadmium removal was 77.81% at a working pH equal to 6, and 99.76% for lead at pH of 5, which is reached after 10 min. It was noted for both lead and cadmium that as the metal concentration increases the amount of metal adsorbed per gram of adsorbent. The experimental data of biosorption of lead and cadmium favourably reproduce Elovich models and pseudo-second order, with correlation coefficients (R^2) for lead 1 and cadmium from 0.9986.

Characterization Techniques

Among the different types of heavy metal bio-absorbents, we have a wide range of analyses that can characterize these compounds and observe their encapsulation power, and their physico-chemical relationship with samples to be absorbed with respect to the bio-absorbents, but there are some techniques that stand out for their ease and depth in characterizing of bio-absorbent and analyte. These efforts are to detect physical and chemical changes in the structure of compounds and thus better understand the phenomena they utilize (Hamza et al. 2019). Among these techniques, we can include scanning electron microscopy (SEM), Fourier transform infrared spectroscopy (FTIR), X-ray diffraction (XDR), thermogravimetric analysis (TGA), and the different adsorption isotherm studies.

Normally it is necessary to analyse which is the group or chemical component in lignocellulosic residues (which in many cases are similar but the quantity varies) and is this the real cause of metal retention. Functional groups such as hydroxyl, carboxyl, sulfhydryl, sulphonate, etc. have been proposed to be responsible for metal sorption binding by different biosorbents, and their importance for uptake depends on factors such as, quantity of sites, accessibility, chemical state, or affinity between metal and site. Analysing the structure of lignocellulosic compounds, cellulose provides 30–50% of the structure as units composed of β-D-glucopyranose

sugars, with approximately 65% of cellulose highly oriented, without leaving access to water or other solvents. On the other hand, hemicellulose and lignin provide between 20–30% and 15–25%, respectively of the remaining biomass. Therefore, it is through these latter groupings that are supposed to interact with the heavy metals. There are also small amounts of water, ash, cyclic hydrocarbons, and organic and inorganic materials present in lignocellulosic sources (Chabannes et al. 2018).

Fourier transform infrared spectroscopy (FTIR) is a valuable technique to identify functional groups present on the surface of the adsorbents before and after the adsorption process. This technique can determine the presence and interaction analysis of certain chemical groups in all samples, such as amino radicals (NH−), carboxyl (−COOH), and hydroxyl (OH−). When FTIR spectra show a strong peak at 3445 cm^{-1}, it represents the –OH stretching of phenol group of cellulose and lignin, and if a peak appears at 2927 cm^{-1}, this indicates the presence of a $–CH_2$ aliphatic compound. The appearance of peaks at 1735 cm^{-1} and 1633 cm^{-1} indicates the presence of C–O stretching of an aldehyde group and C–C stretching of a phenol group, respectively. Similarly, the peaks between at 1508 cm^{-1} and 1372 cm^{-1} in the spectrum of a bio-absorbent can be due to C=C of aromatic ring. After adsorption, the shifting of –OH and the slight decrease in intensity indicate the involvement of OH in the adsorption phenomena. Scanning electron microscopy (SEM) is performed in order to obtain information about the surface morphologies of un-activated, activated and activated with metals-loaded adsorbent, at different magnifications, and to enhance the electron conductivity of the samples, it can be done by coating with gold particles. The particle size(s) and Polydispersity Index of adsorbent before accumulation of metal were determined using zeta-sizer (Zetasizer). X-ray diffraction (XRD) spectra are performed to determine changes in the structure of bioadsorbents that can help determine the existence of interactions between heavy metals and biosorbents. Thus, because of the amorphous nature of biosorbent compounds it yields complex spectra, with no defined peaks in the absence of metals. On the contrary, when we have absorption of heavy metals, defined peaks appear, characteristic of the crystalline structures of heavy metals inserted in a mixture of complex peaks of an amorphous structure (Noli et al. 2019).

Also and complementary to the above methods, thermogravimetric analysis (TGA) is used for the characterization of thermal degradation of adsorbent before and after metal accumulation. In addition, it is used to measure the material's thermal stability and the rate of change of weight of a sample as a function of time and temperature in a controlled atmosphere. It is primarily used to determine the thermal and/or oxidative stability of materials as well as their compositional properties. The weight of a sample is recorded as a function of temperature under air or inert atmosphere, such as helium or argon. To slow down the oxidation, the measurement is performed under a lean oxygen atmosphere (1–5% O_2 in N_2 or He). To obtain information about the elemental compositions of the biosorbents, the carbon (C), hydrogen (H), nitrogen (N) and sulphur (S) contents of each sample are measured by using a CHNS Analyzer. The percentage of oxygen is calculated by subtracting the C, H, N, and S contents from 100%. Subsequently, the adsorption studies are also focused on determining the effect of the presence of one adsorbate on the

adsorption of a second adsorbate. The adsorption isotherms are usually modelled by using the Langmuir and Freundlich isotherm models (Wang et al. 2019). A summary of different characterization techniques using agro-waste materials is shown in Table 11.1.

Modelling

Parallel to the extensive experimental activity carried out during the last decades on heavy metal biosorption, several mathematical models, most in the form of empirical correlations, have been developed to elucidate and represent the heavy metal adsorption on biomass binding sites (Volesky and Schiewer 2000). Mathematical modelling represents a useful tool to describe the complex mechanisms characterizing the biosorbent and the solute interactions and assists in the optimization and design of biosorption processes. The biosorption models are classified into two main categories based on the mode of operation (batch or continuous) used to conduct the process. Although most industrial applications prefer a continuous mode of operation, batch experiments have to be used to evaluate the required fundamental information, such as biosorbent efficiency, optimum experimental conditions, biosorption rate and possibility of biomass regeneration.

Batch System

Equilibrium Study

Biosorption process generally started with batch mode, this experiment compares the biosorption capacity (q_e, mg.g^{-1}) and percentage of removal (%) versus the residual concentration of the pollutant in the solution at equilibrium, Eqs. (11.1) and (11.2):

$$q_e = \frac{(C_0 - C_e)V}{m} \tag{11.1}$$

$$\text{Removal}(\%) = \frac{(C_0 - C_e)100}{C_0} \tag{11.2}$$

Where C_0, C_e are the concentration of pollutant in the initial solution and at equilibrium in the aqueous phase after adsorption (mg.L^{-1}), V is the volume of the solution (L), and m is the mass of the biosorbent (g).

The main operating factors are evaluated in order to optimize the experimental conditions (solution pH value, biosorbent dose, initial sorbate concentration,

Table 11.1 Different characterization techniques results done by various researchers using agro-waste materials

Biosorbent	Technique	Analysis	Reference
Coffee residue	Adsorption isotherms	The BET surface area was determined by means of the standard BET equation applied in the relative pressure range from 0.06 to 0.3 m^2/g	Boudrahem et al. (2011)
	Thermogravimetric analysis (TGA)	Raw coffee residue exhibits only one prominent wave of weight loss [between 200 and 400 °C] with a maximum centred at 270 °C, followed by a slow weight loss with decreasing rate. A considerably different pattern is exhibited by the H_3PO_4-treated lignocellulosic material. Through this temperature range of 400–900 °C, two DTG peaks appear with maxima at 525 °C and 700 °C. Thus, impregnation with H_3PO_4 brings about considerable effects on the course of pyrolysis of coffee residue: (i) it shifts degradation to considerably higher temperatures, (ii) it enhances the early dehydration stage combined with an evolution of low-boiling volatiles, (iii) it strongly retards the evolution of volatiles where up to 600 °C only around 50% weight is lost, and (v) it promotes the carbon yield. These observations suggesting mechanism, involving dissolution of some chemical components with bond cleavage, followed by recombination at other sites forming new polymeric structures that are thermally more resistant	
	Infrared spectra of the Fourier transform (FTIR)	FTIR spectra present for the activated carbon impregnated with H_3PO_4 (50% optimal chemical ratio). They show the following bands: 4000 cm^{-1} and 3500 cm^{-1} correspond to the –OH groups of the phenol function; 2906 cm^{-1} and 2847 cm^{-1} correspond to stretching C–H groups of aliphatic, olefinic, and aromatic structures; 1556 cm^{-1} is attributed to stretching C=O of the carbonyl groups in quinine as well as γ-pyrone structure; and 1424 cm^{-1} corresponds to stretching C–O or O–H deformation in carboxylic acids	
Palm shell	Adsorption isotherms	The BET surface area was found to be 0.2979 m^2/g	Sreelatha et al. (2010)
	X-ray diffraction (XDR)	The X-ray diffraction pattern shows a peak centred around 21° corresponding to a 002 reflection of disordered packing of micrographites. The peak is broad and suggests an amorphous structure. The peak at 21° corresponds to an interlayer distance of 0.423 nm which suggested a disordered carbonaceous interlayer.	

(continued)

Table 11.1 continued

Biosorbent	Technique	Analysis	Reference
	Infrared spectra of the Fourier transform (FTIR)	Possible interactions of pre-treated with sulphuric acid (APSP) and dye was studied by comparing the features of the spectra obtained from IR spectroscopy studies of dye, dye-loaded, and dye-unloaded APSP. APSP showed a broad frequency at ~3419.42 cm^{-1}, which can be assigned to N–H/–OH stretching. After the adsorption of the dye molecule the peak is shifted to 3424.65, 3383.76, and 3174.57 cm^{-1} for AO-II, DSB, and AV-7 dyes, respectively. The peak at ~1625.29 cm^{-1} was assigned to the N–H bond of amine or characteristics of the elongation of the aromatic –C=C- bonds which also have been shifted to 1617.62, 1608.24, and 1609 cm^{-1} for AO-II, DSB, and AV-7 dyes, respectively. The peak at 1378.58, which corresponds to C–N stretching, is missing after the adsorption of dye molecules. The peak at 1200 cm^{-1} is associated with the C–O stretching of the aromatic ring which is also shifted to a lower frequency region	
	Scanning electron microscope (SEM)	The morphology of APSP was studied using a scanning electron microscope. The surface is magnified 1000 times which shows that the adsorbent has an irregular, rough, and porous surface with identifiable micropores and mesopores	
Corncob and peanut shell precursors	Adsorption isotherms	The BET surface area was found to be 862 m^2/g and 654 m^2/g for corncobs-based or peanut shells–based activated biocarbons, respectively	Wiśniewska and Nowicki (2019)
	Viscosity	Polyacrylic acid (PAA) with the weight average molecular weight equal to 2000 Da	
	Zeta potential (ZP)	The electrophoretic mobility of the solid particles (in the absence of adsorbates) takes negative values, and it is not possible to determine the isoelectric point (IEP) value. In the case of both activated carbons, the addition of Pb(II) cations causes a noticeable decrease in the absolute values of electro-kinetic potential, which probably results from the accumulation of their positive charges at the stiff and mobile parts boundary	
	Scanning electron microscope (SEM)	The small, bright fragments, which can be observed in both SEM images, may be a consequence of the mineral matter presence in the porous structure of the studied samples. The mean pore size of both activated carbons equal to approx. 2.5 nm determines the penetration of PAA macromolecules into their interiors. This is confirmed by the SEM images. In such a case the separation of these aggregates containing activated carbon and binding hazardous adsorbates is facilitated	

Chitosan (CH) and thiobarbituric acid (TBA) to form chitosan/thiobarbituric acid (CT)	Ultraviolet-visible (UV-Vis) spectroscopy analysis	UV analysis. The electronic absorption spectra of chitosan/thiobarbituric acid exhibited an absorption maximum at 226 nm, which can be assigned to the $\pi \rightarrow \pi^*$ transition, whereas the absorption bands at 282 and 363 nm can be assigned to $n \rightarrow \pi^*$ intra-ligand transitions	Bhatt et al. (2018)
	Infrared spectra of the Fourier transform (FTIR) analysis	FTIR analysis showed that intense broadbands in the 3300–3500 cm^{-1} region can be attributed to N−H and the O−H stretching vibrations in chitosan/thiobarbituric acid (CT). The absence of peak at around 3600 cm^{-1} can be attributed to the keto-tautomer of thiobarbituric acid, evidencing the formation of CT. Furthermore, there were either slight shifts in characteristic peaks of CT or change in intensities after adsorption of mercury species. The amide III band shifted from 1319 cm^{-1} in CT to ~1304, 1302, and 1301 cm^{-1} in CT–Hg^0, CT–Hg_2^+, and CT–CH_3Hg^+, respectively	
	Scanning electron microscopy–energy-dispersive X-ray (SEM–EDX) analysis	The EDX spectra showed the presence of sulphur in CT, indicating the incorporation of 2-thiobarbituric acid into chitosan. Furthermore, the presence of mercury peaks after adsorption of inorganic, methyl, and elemental mercury confirmed the adsorption of all of the three mercury species onto CT	
	Nuclear magnetic resonance (NMR) analysis	The NMR spectrum of CT and proposed structure of CT, respectively. The peaks at 2.05–2.07 ppm were attributed to the three methyl protons of N-acetyl glucosamine, and those at 3.18 ppm, to the 2 protons (H_2) of glucosamine. The overlapping signals from 3.7 to 3.9 ppm were attributed to protons connected to the nonanomeric C3−C6 carbons in the glucopyranose ring of chitosan chain, and the signal at 5.029 ppm was attributed to the anomeric proton and to the proton connected to C5 of the pyrimidine ring of thiobarbituric acid	
	Differential scanning calorimetry (DSC) analysis	Differential Scanning Calorimetry (DSC) analysis curves showed two exothermic peaks at 279 °C and 302 °C in CH and 285 °C and 301 °C in CT were attributed to the thermal decomposition of amino residues. Furthermore, no exothermic peak was observed at around 400 °C, thereby indicating that the N-acetyl groups were not present on the polymer matrix and only amino residues were observed, which are less thermally stable than the N-acetyl.	

(continued)

Table 11.1 continued

Biosorbent	Technique	Analysis	Reference
	Thermogravimetric analysis (TGA) analysis	Thermogravimetric analysis (TGA). Both CH and CT exhibited similar thermal behaviour. The weight loss in the 40–100 °C region was due to the loss of adsorbed water or that absorbed in the inner polymeric network. The weight loss that occurred at ~200–300 °C was slightly less in CT as compared to that in CH, which could be due to the supramolecular cross-linking of thiobarbituric acid in the polymer structure, leading to slower thermal degradation of the biopolymer. The weight loss observed at 300–400 °C can be ascribed to degradation of polysaccharide units and breakdown of the glucopyranose ring. The weight loss in the 400–500 °C range could be due to emission of volatile products, such as CO and CO_2, and the formation of the carbon residue.	
	X-ray diffraction (XRD)	X-ray diffraction (XRD) analysis of CH, CT, and mercury-loaded CT samples. The XRD pattern of CT showed a broad peak at around $2\theta = 20°$, indexed as the 101 plane of crystal form I, which is present due to the amorphous state of chitosan. The higher peak intensity for CT at 19.93° could be attributed to the intermolecular hydrogen bonding patterns and crystalline structure. Furthermore, the position of the peak at 19.93° for CT shifted to 21.95°, 19.98°, and 20.27° on interaction with Hg^0, Hg^{2+}, and CH_3Hg^+, respectively. Furthermore, the binding of the sulphur species with Hg^0, Hg^{2+}, and CH_3Hg^+, respectively, was also supported with the generation of new peaks at 46.55, 41.21, and 42.73°, respectively. The crystalline index was calculated to be 50.07% using crystalline index (%) = $[(I_{100} - I_{am})/I_{110}]x100$, where I_{100} denotes the maximum intensity at ~20° and I_{am} is the intensity of amorphous diffraction at 16°, whereas the crystallite size was found to be 1.24 nm for the peak at 19.939° using Scherrer's expression	
	X-ray photoelectron spectroscopy (XPS)	X-ray photoelectron spectroscopy (XPS) analysis. In CT, the binding energy at 164.6 eV corresponded to organically bound sulphur. The typical S $2p_{3/2}$ binding energy for unbound thiols was between 163 and 164 eV, suggesting that the thiol group of thiobarbituric acid is free after layering with chitosan. After the adsorption of Hg(II), the appearance of peak at 161.7 eV suggested binding of thiol group to mercury, whereas the peak at 163.2 eV corresponded to the free thiol group. Similar signals were observed after adsorption of elemental mercury and methyl mercury	

Orange peel	Infrared spectra of the Fourier transform (FTIR)	The orange peel FTIR spectrum showed the peak of the hydroxyl group (–OH) ranges from 3424 to 3450 cm^{-1}, the C=O bond of non-ionic carboxylic acids in the range 1735–1750 cm^{-1}, the symmetric and asymmetric bonding of C=O vibration of ionic carboxylate group in the range of 1617–1637 cm^{-1}, and the symmetrical vibration of ionic carboxylic group in the range of 1300–1500 cm^{-1}. The peak that appears in the 3440 cm^{-1} shows the presence of free hydrogen or the O–H bond in alcohols, phenols, and carboxylic acids present in pectin, cellulose, and lignin. This peak has changed 8 units in the orange peel after absorption, which indicates effect of this group on the absorption of thorium. Due to the FTIR spectrum of orange peel, the effect of hydroxyl and carboxylic groupings, that are abundantly present in this adsorbent, is known in the biosorption of thorium. The absorption of thorium on orange peel is most likely due to the electrostatic attraction between these functional groups and the metal cation. The carboxylic group loses proton at high pH ($–COO^-$) and has a negative superficial potential, which increases the metal cation absorption capacity	Gh et al. (2018)
	X-ray fluorescence (XRF)	The results show that the percentage of calcium and potassium ions decreased significantly after adsorption, and on the other hand, with the adsorption of thorium, the percentage of thorium in adsorbent after absorption increased (93% by weight). So, calcium and potassium ions are replaced by thorium ions during the adsorption process. By measuring the concentrations of calcium and potassium ions in samples taken from the column outlet solution can also study the same mechanism of the process	
Tangerine peel	Infrared spectra of the Fourier transform (FTIR)	As can be seen for untreated tangerine peel, a broad absorption peak around 3400 cm^{-1} indicates the existence O–H stretching vibrations occur within a broad range of frequencies, indicating the presence of ‘free’ hydroxyl groups and bonded O–H bands of carboxylic acids. After-chemical treatment resulted in shifting of this peak towards higher value of wave numbers (around 3430 cm^{-1}), which corresponds to polymorphic form of cellulose. Also, for untreated peel, peak of medium intensity in the area of carbonyl group, around 1740 cm^{-1}, can be attributed to acetylene and uronic ester groups of pectin, lignin, and hemicelluloses or to ester bonding of carboxyl groups from ferulic and coumaric acid of lignin and hemicelluloses	Memić et al. (2018)

(continued)

Table 11.1 continued

Biosorbent	Technique	Analysis	Reference
Wheat straw	Infrared spectra of the Fourier transform (FTIR)	Ground, dried wheat straw (*Triticum aestivum*) was subjected to FTIR analysis for its characterization in terms of functional groups (adsorption sites). The characteristic functional group present in wheat straw was C=O (1650.8 cm^{-1})	Ali et al. (2011)
Sugarcane bagasse	Ultraviolet-visible (UV-Vis) spectroscopy analysis	The absorbance calculated of lignin solution at 280 nm. Furthermore, furfuraldehyde and hydroxymethylfurfural in the acid solution were quantified by HPLC. The conversion factor for furfuraldehyde and hydroxymethylfurfural into cellulose and hemicellulose are 1.37 and 1.29, respectively	Rocha et al. (2015)
	Determining the amount of carbohydrates by HPLC	The amounts of cellobiose, glucose, xylose, arabinose and acetic acid present in the acid hydrolysate of lignocellulosic materials were quantified by HPLC. The concentrations of glucose and cellobiose were converted into cellulose, concentrations of xylose and arabinose were converted to hemicellulose, and concentration of acetic acid was converted to acetyl groups. The masses were divided by the dry weight of the original material and multiplied by the hydrolysis factor: 0.90 and 0.95 for glucose and cellobiose to cellulose, respectively; 0.88 for xylose and arabinose to hemicelluloses and 0.72 for the conversion of acetic acid to acetyl group	
	Elemental analysis	The content of carbon, hydrogen, nitrogen and sulphur was determined in an element analyzer. The oxygen content was determined by the difference. As average, the bagasse samples contained 42.2% of cellulose, 27.6% of hemicelluloses, 21.6% of lignin, 5.63% of extractives and 2.84% of ashes. In general, the composition of these values is also within the ranges state, which are 40–50% for cellulose, 25–30% for hemicelluloses, and 20–25% of lignin. (Lignin is thought to be linked mainly to side-chain sugars present in the hemicelluloses, as arabinose and galactose)	

Carica papaya	Infrared spectra of the Fourier transform (FTIR) biosorbent	The FTIR spectrum of raw biomass showed several distinct and sharp absorptions at 3409 cm^{-1} (indicative of primary amide, $–CONH_2$ group), 2925 cm^{-1} (indicative of –CH stretching), 2359 cm^{-1} (indicative of = $N–H_2^+$ group), 1742 cm^{-1} (indicative of five ring lactone), 1627 cm-1 (indicative of amide I band of amide bond in N-acetyl glucosamine polymer or of the protein peptide bond), 1439 cm^{-1} (indicative of the bending of CH_2CH_3), and the band at 1036 cm^{-1} (indicative of sulphur compounds, S=O). The FTIR spectra of papaya wood exposed to Hg(II) ions indicated no shifts or change in any of the characteristic absorbance bands present in raw biomass with the exception of a peak shift at 3434, 2362, and 1645 cm^{-1}. The spectra exhibited absorptions at approximately 3434 cm^{-1}, suggesting the occurrence of secondary amide, –CONH–. The results implied mainly involvement of amide groups in sorption of Hg(II) ions. Although slight changes on the other absorption frequencies were observed	Basha et al. (2008)
	Scanning electron microscopic (SEM)	Electron micrographs of the raw and Hg(II) sorbed biomass of *C. papaya* clearly distinguish two cases. The surface of raw biomass is rough and irregular with a large area for metal–surface interaction which formed a cage like structure after Hg(II) sorption. The exact reason for this formation is not known at this moment; however, the chemical interaction between functional groups of the biomass and mercury ion may be responsible for the formation of cage-like structures. Energy-dispersive X-ray analysis (EDX) provides elemental information through analysis of X-ray emissions caused by a high-energy electron beam. The spectra recorded in spot profile mode indicate the presence of C, N, O, Al, Na, K, and S. These signals are due to X-ray emissions from the fibre and proteins present on the cell wall of the biomass. Additional signals of Hg are noted, indicating the binding of metal ions on the biomass. Moreover, for the sample after biosorption, was observed on the EDX spectrum that the peaks of K disappeared. This observation could suggest that the mercury species has replaced K^+ on the cell wall of *C. papaya*, thereby signifying an ion-exchange mechanism as one of the mechanisms of Hg(II) biosorption for this biosorbent	
	Atomic absorption spectroscopy (AAS)	The pH for all experiments was 5.0 except for effect of pH where the pH was varied from 3.0 to 8.0. This is irrespective of the pH PZC (6.25) to avoid metal ion precipitation	Gilbert et al. (2011)

(continued)

Table 11.1 continued

Biosorbent	Technique	Analysis	Reference
Tamarindus indica seed powder (TSP)	Infrared spectra of the Fourier transform (FTIR)	*Tamarindus indica* seed powder (TSP) mainly contains polysaccharide with fats, tannins, proteins and amino acids in minimum proportion. The FTIR spectra of TSP shows the presence of several functional groups, indicating the complex nature of TSP. The broad and strong band at 3450 cm^{-1} suggests the presence of OH and NH2 groups. The peak at 2904 cm^{-1} can be attributed to CH stretching vibrations while the peak appearing at 1652 cm^{-1} arises from CO stretching in amide groups. The peak at 1465 cm^{-1} represents CH3. The peak around 1160 cm^{-1} indicates CN stretching vibration. The peak at 1060 cm^{-1} corresponds to CO stretching vibration of alcohols and carboxylic acids. After Cu(II) biosorption, the band at 3450 cm^{-1} corresponding to OH and NH groups shifts to the lower frequency (3390 cm^{-1}). Thus, it can reasonably be concluded that OH and NH_2 groups may be the main binding sites for Cu(II) onto TSP. Also, the peaks at 1652 cm^{-1} and 1060 cm^{-1} shift to 1615 cm^{-1} and 1030 cm^{-1} respectively. This shift in peaks suggests that CO and CO groups participate in the Cu(II) binding process. Hence, FTIR spectral analysis reveal that functional groups like NH_2, OH, CO, and CO present on TSP surface are involved in Cu(II) biosorption	Chowdhury and Saha (2011)
	Scanning electron microscopic (SEM)	SEM is one of the most useful tools for studying the surface morphology of a biosorbent. The SEM images of native TSP and Cu(II)-loaded TSP. SEM image of TSP before metal biosorption shows a rough, uneven and heterogeneous surface with porous structure. The rough surface can help increase the surface area available for biosorption of Cu(II). However, the porous textural structure is not observed on the surface of Cu(II)-loaded TSP. The surface morphological change can be linked to precipitation/complexation of Cu(II) on the biosorbent surface	
	Adsorption isotherms	The BET surface area, total pore volume and average pore diameter of the biosorbent before metal biosorption was found to be 29.46 m^2/g, 0.0189 cm^3/g, and 67 Å, respectively.	
	X-ray diffraction (XRD)	The XRD pattern of TSP and Cu(II) loaded TSP. The XRD pattern of TSP does not show any characteristic peaks indicating amorphous nature of the biosorbent. The amorphous nature suggests that metal ions could easily penetrate into the surface of the biosorbent as was observed in the case of gum kondagogu. The XRD pattern of metal-bound TSP shows distinct and complex peaks, indicating the deposition of Cu(II) on the surface of TSP	

Citrus maxima peel (CM), passion fruit shell (PF), and sugarcane bagasse (SB)	Scanning electron microscopic (SEM)	The biosorbents used in this study uptake metal ions through complexation or ion exchange processes, which might be influenced by the surface properties of the test biosorbents. SEM micrographs with valleys and peaks exhibiting the roughness of CM and PF and the absence of protrusions for SB. In the SEM images, the biosorbents exhibited limited pore volume and are not porous. The biosorbents uptake metal ions through the functional groups on their surfaces. The pore volume and specific surface area are less crucial than the BET surface area, ZP, and pH values of the biosorbents. The specific surface area of the biosorbent was lower than 2 m^2/g. The results demonstrated that the pore volume and surface area are not critical in this study	Chao et al. (2014)
	Infrared spectra of the Fourier transform (FTIR) biosorbent	FTIR spectroscopy was used to determine the functional groups before and after adsorption present at the biosorbent surface. The spectra are similar before and after adsorbing Cu^{2+}. The broad absorbance at 3200–3600 cm^{-1} indicates the presence of OH or COOH groups. A weak absorbance at 1690–1760 cm^{-1} suggests the presence of the C–O group. The absorbance band at 1200–1220 cm^{-1} might result from the CO and OH groups in COOH, and the absorbance at 1050–1300 cm^{-1} might result from the C–O group on the surface. Thus, the FTIR spectra indicate that the biosorbent surfaces are rich in polymeric hydroxyl groups, CHN and COO groups, and OH groups of polysaccharides. Agricultural by-products usually are composed of lignin and cellulose and other functional groups of lignin (i.e. alcohols, aldehydes, ketones, carboxylic, phenolic and ether groups), which all have the ability to some extent to bind heavy metals by donation of an electron pair from these groups to form complexes with metal ions in aqueous solution	

(continued)

Table 11.1 continued

Biosorbent	Technique	Analysis	Reference
	Zeta potential (ZP)	The biosorbent zeta potentials (ZP) for various pH values determine the ion exchange potential. A negative ZP indicates a negative surface charge on the adsorbent surface, and vice versa. Significantly, the table shows negative ZP values for the entire pH range tested. Thus, metal ions may adsorb to the biosorbent surface by an ion-exchange mechanism. The results demonstrated that ion exchange is one of the adsorption mechanisms for metal ions in the test biosorbents. The cation-exchange capacities (CEC) values of the biosorbents arise from the functional groups present on their surfaces. The CEC values of the CM, SB, and PF are 47.3, 11.8, and 26.9 (meq/100 g), respectively. The dissociation of hydrogen ions or other cations from a functional group under specific pH conditions generates an exchangeable cation. Functional groups such as carboxyl, amino, and hydroxyl on the surface of the biosorbents provide complexation sites for metal ions. Groups containing oxygen or nitrogen atoms provide nonbonding electrons for coordination with the divalent metal's ions. Thus, the surface functional groups are the dominant factors in determining adsorption capacity. According the main element composition of the biosorbents, which predominantly contain carbon and oxygen, and no nitrogen, consequently amino groups are not present in substantial quantities, whereas carboxyl and hydroxyl groups are the potentially dominant groups	
Cashew nut shells	Thermogravimetric analyzer coupled with a Fourier transform infrared spectrometer (TG-FTIR)	The volatile pyrolysis product species identified in this study are (i) carbon monoxide (CO); (ii) carbon dioxide (CO_2); (iii) tar (by difference using gravimetric data); (iv) water (H_2O); (v) methane (CH_4); (vi) ethylene (C_2H_4); (vii) formaldehyde (CH_2O); (viii) formic acid (HCOOH); (ix) carbon sulphide (COS); (x) acetic acid (H_3CCOOH); (xi) methanol (CH_3OH); (xii) ammonia (NH_3); (xiii) hydrogen cyanide (HCN); (xiv) isocyanic acid (HCNO); (xv) acetone (H_3COCH_3); (xvi) phenol (C_6H_5OH); and (xvii) acetaldehyde (H_3CCHO). Tar evolution patterns and yields were determined by difference, using the sum of gases quantified by FTIR and the balance curve obtained thermogravimetrically	Tsamba et al. (2007)

Olive cake	Elemental analysis CHNS (this technique consists of the determination of the percentage of C, H, N and S)	The elemental analysis of the biosorbent. The sample was mainly composed of carbon (51.57%) and oxygen (35.33%). If the results are compared with the ones obtained in previous studies of the untreated olive cake, it was observed that the carbon content was concentrated after the washing, whereas the oxygen content was reduced. The nitrogen, hydrogen and sulphur contents remained almost constant after the treatment. The concentration of carbon could be due to the elimination of inorganic compounds as it showed the reduction of ash that occurred after the treatment. The reduction of oxygen could be due to the elimination of water caused by the drying carried out. The elemental analysis showed similar results to the ones obtained by other authors for hydrolysed live cake. On the other hand, the proximate analysis. In this case, as aforementioned, ash and moisture contents were reduced with respect to untreated olive cake. The volatiles were the major compounds present in the sample (70.08%)	Fernández-González et al. (2018)
	Differential scanning calorimetry (DSC) analysis	The first peak of DTG curve appeared at temperatures around 100 °C, corresponding to the moisture content and the external moisture bounded by the surface tension. The second peak appeared at a temperature around 280 °C, corresponding to the decomposition of hemicellulose. Another peak was observed around 380 °C, which could be attributed to cellulose. Those two peaks appeared for the hydrolysed olive cake and not for the untreated olive cake. In the untreated one, it appeared as one broad peak whereas in the washed sample it appeared as two peaks which have slightly shifted to the right with respect to the untreated sample. It could be because leaching promoted the thermal stability of the material. The degradation of lignin occurred in a broad range of temperatures, appearing as a baseline of the DTG curve and not as a well-differenced peak	
Olive stone and sugar cane bagasse	Elemental analysis CHNS (this technique consists of the de termination of the percentage of C, H, N and S)	Characterization of a biosorbent is an important analysis for understanding the behaviour or the mechanism of cadmium removal on the surface of biosorbent. These in order to quantify the amount of C, H, N, S and O by to elemental analysis and the moisture content of olive stone and bagasse by-products. Elemental analysis results showed that olive stone and bagasse have a similar elemental composition, being composed mainly of carbon (51.78% and 48.57% for olive stone and bagasse, respectively) and oxygen (41.77% and 45.58% for olive stone and bagasse, respectively). The H concentration was 6.33% and 5.41% for olive stone and bagasse, respectively. There is no sulphur on both olive stone and bagasse. The moisture content was lower than 5% for both biosorbents	Moubarik and Grimi (2015)

(continued)

Table 11.1 continued

Biosorbent	Technique	Analysis	Reference
	Infrared spectra of the Fourier transform (FTIR)	FTIR analysis is primarily used to identify the chemical groups present in the biosorbents. FTIR spectra before Cd^{2+}biosorption. Direct information on the presence of surface functional groups can be obtained from FTIR studies. FTIR results revealed very similar spectra for olive stone and bagasse, which confirmed that both have similar functional groups. In order to illustrate the distinct attributions, the corresponding assignments identified for the olive stone and the bagasse. The FTIR analysis shows the absence of nitrogen and sulphur groups in the olive stone and the bagasse structure, whereas we note the presence of different oxygen groups, mainly carbonyl, alcohol and phenol groups, ethers and esters. Hence, the good sorption properties of the olive stone and bagasse towards Cd^{2+} ions can be attributed to the presence of these functional groups	
	Adsorption isotherms	The results show that the olive stone pores are mesopores while bagasse pores are macropores. The average pore diameter of olive stone and bagasse was found to be 12.7 nm and 57.2 nm, respectively. The specific surface area of olive stone and bagasse is 0.378 m^2/g and 0.487 m^2/g, which was supported by the data reported in other researches. The strong interaction between adsorbate molecules and pore walls further controls the filling of micropores during adsorption process	
	Zeta potential (ZP)	Zeta potential is the manifestation of surface charge density of the adsorbent. Surface charge density has a significant effect on Cd^{2+} metal ions adsorption on olive stone and bagasse. It obtained the variation of zeta potential of olive stone and bagasse as a function of pH and the pH at the point of zero charge (pH_{pzc} of olive stone is 4.2 and pH_{pzc} of bagasse is 5.7), similar results have been reported by other researchers. The pH_{pzc} value is the point at which surface functional groups do not contribute to the pH of the solution. Above this pH value, the surface charge becomes negative and the adsorbent will take up the cations with higher affinity	

	Scanning electron microscopy (SEM)	Olive stones and bagasse by-products used in this study were analysed by SEM in order to examine their morphology. The SEM image of olive stones and bagasse before cadmium adsorption show that pores of different sizes and different shapes could be observed. As shown in these images, the prepared olive stones and bagasse have irregular structure, which can favour the biosorption of Cd^{2+} ions on different parts of biosorbent. These images confirm the previous results obtained by the analysis of the porosity of olive stones and bagasse	
Soya bean	Infrared spectra of the Fourier transform (FTIR)	The FTIR spectra of soya bean as an adsorbent of Pb and As show before and after biosorption of heavy metal respectively. A broad band between 3201 and 3518 cm^{-1} in both adsorbents is indicative of the presence of free and hydrogen-bonded OH groups on adsorbent surface. This stretching is due to both the silanol groups (Si–OH) and adsorbed water (peak at 3400 cm^{-1}) at the adsorbent surface. The stretching of OH groups bound to methyl groups shows a signal between 2852 and 2924 cm^{-1}. Similarly, peaks at 1743 and 1317 cm^{-1} are indicative of carboxyl group, while those at 1539.20 and 1458.18 cm^{-1} are indicative of $–CH_2$ and $–CH_3$ groups. The peak at 1251, 1035, 896, and 850 cm^{-1} is due to $–SO_3$ stretching, C–O stretching, C=O stretching, and aromatic –CH stretching. The presence of polar groups on the surface of adsorbent is likely to give considerable cation-exchange capacity to the adsorbents. The peaks at 783 cm^{-1} indicate the presence of Si–H	Gaur et al. (2018)
	Field emission gun scanning electron microscopes (FEG-SEM)	The SEM micrograph of un-activated, activated and activated metals (Pb and As)-loaded adsorbent. As mentioned previously, the activated adsorbent contains exposed cavities and pores which favour the adsorption of metals. From it could be inferred that surface texture of the soya-based adsorbent changes drastically after the adsorption of the heavy metals. The surface of the soya-based biosorbent also appears uneven and irregular with cavities which facilitate interaction of heavy metals (Pb and As) with the biosorbent surface, leading to proper metals adsorption. An alternation in rough surface was examined after the use of Pb and As in the adsorption studies	

(continued)

Table 11.1 continued

Biosorbent	Technique	Analysis	Reference
	Dynamic light scattering (DLS) Zeta meters	The instrument Zetasizer uses the phenomenon of dynamic light scattering to reveal the particle size of the sample through the measurement of Polydispersity Index. The dynamic light-scattering measurement shows polymer particles around 0.1 μm with a polydispersity of 7. Particles in suspension/solution undergo Brownian motion which is induced by the bombardment of the solvent particles that moves due to their thermal energy. When the laser light hits the particle surface, the smaller particles move faster as the rate of intensity of light is directly proportional to the size of particle. Also, the movement of the particle depends on the motion of solvent molecule	
	Thermo-gravimetric analysis (TGA)	Thermal stability of soya waste–based bioadsorbent is directly dependent on decomposition temperature of its various oxides and functional groups. The surface groups present on carbons moiety and those formed as a result of interaction with oxidizing gases or solutions are generally quite stable even under vacuum at temperatures below 150 C, irrespective of the temperature at which they are formed. However, when the carbons are heated at higher temperatures, the surface groups decompose, producing CO (150–600 C), CO_2 (350–1000 C), water vapour and free hydrogen (500–1000 C). The principal experimental variables which could affect the thermal degradation characteristics in air and nitrogen flow in a TG experiment are the pressure, purge gas flow rate and the weight of sample. In the present study, the operating pressure was kept slightly positive; the purge gas flow rate was maintained at 200 C	
Core–shell structured biosorbent derived from chemical-mechanical pulp (CMP) and carboxymethylated cellulose fiber (CMF)	Infrared spectra of the Fourier transform (FTIR)	The differences of functional groups between original CMP and the as-prepared CMF. Obviously, the spectra showed that the broad bands appeared at around 3250–3500 cm^{-1} was consistent with the hydroxyl groups; meanwhile, the signal at roughly 2920 cm^{-1} may be due to the C–H stretching vibration. The broad peak at 1064 cm^{-1} can be attributed to the stretching vibration of C–O–C. Comparing the spectrum of CMP with that of CMF, the peaks at 1600 cm^{-1} and 1400 cm^{-1} were related to the C=O stretching and bending vibration, respectively. The results confirmed that –COOH was successfully introduced into CMF	Wang et al. (2019)

	Scanning electron microscopes (SEM) and laser scanning confocal microscope (LSM)	In the process of carboxymethylation, lignin would wrap on the surface of the CMF like a 'shell' and prevent the swelling of CMF. Figure 11.3c shows the different fluorescence intensity of the cross-section of CMFs after dyed with anionic fluorescent brightener. We found that the surface of the as-prepared CMF showed a strong fluorescence (white) while the internal exhibited a weak fluorescence (dark), which was mainly due to the core–shell structure of CMF and the different electrostatic repulsion between the lignin–cellulose constitution and fluorescent brightener. Compared with the lignin-based shell of CMF, he cellulose-based core with more negative charges had a stronger electrostatic repulsion and a less adsorption capacity toward fluorescent brightener, thus leading to the weak fluorescence in the internal.	
	X-ray diffraction (XRD)	XRD shows the characteristic peaks of cellulose I present in the CMP samples were 14.8° and 22.5°, respectively. For CMF, a new peak appeared at 21°, which was a typical peak for cellulose II, indicating that high sodium hydroxide concentration could change the cellulose crystal form during the process of carboxymethylation.	
Banana peels waste	Infrared spectra of the Fourier transform (FTIR) biosorbent	FTIR spectra of banana peels particles with a particle size of <250 μm (before and after the pre-treatment stage) were analysed and it shows number of peaks that indicate a complex nature of these particles. It is apparent from this figure that the following peaks 1735–1559 cm^{-1}, 1531.5–1409 cm^{-1}, and 1413.6–1024 cm^{-1} were shifted due to the pretreatment stage. The peaks 1735–1559 cm^{-1}, 1531.5–1409 cm^{-1}, and 1413.6–1024 cm^{-1} were assigned as C=O stretch, C=C stretch, and C=N stretch, respectively. However, the peak of 2326–2048.9 cm^{-1} that was attributed to the OH stretch was not shifted.	Al-Mohammedawi et al. (2019)
	Scanning electron microscopes (SEM)	SEM showing the surface morphology of banana peels particles before and after the pretreatment stage show that microporous structure and rough texture were observed for this sample, which can enhance the performance of banana peels particles as biosorbents. Similar observations were also previously reported when using banana peels as treatment agents. After pre-treatment stage, it was observed that the porous structure of banana peels particles was increased, and the binding sites were occupied. This can be attributed to the adsorption of ammonium, in addition to the possible transfer of carbon compounds from banana peels particles into brewery wastewater.	

temperature). Different isotherm model equations are used to study the biosorption equilibrium, of which the Langmuir and Freundlich are probably the most widely used with a high rate of success.

Langmuir isotherm. Biosorption takes place at specific homogeneous sites on the surface of the biosorbent forming monolayer coverage and the molecule adsorption capacity on one site is independent of its surroundings Eq. (11.3):

$$q_e = \frac{q_m K_L C_e}{1 + K_L C_e} \tag{11.3}$$

where q_m is the maximum binding capacity ($mg.g^{-1}$), and K_L is the Langmuir constant that represents affinity between the sorbent and sorbate through to the free energy of biosorption ($L.mg^{-1}$).

Freundlich, is empirical model, and assumes a multilayer biosorption on a heterogeneous surface with no uniform distribution of heat of adsorption Eq. (11.4):

$$q_e = K_F C_e^{1/n} \tag{11.4}$$

where K_F is a constant relating the biosorption capacity ($mg.g^{-1}$)($L.mg^{-1}$)^n and $1/n$ is a dimensionless empirical parameter relating the biosorption intensity, higher the $1/n$ value, more favourable is the adsorption, which varies with the heterogeneity of the material and when $n = 1$, all sorption centres are equivalent. The model is widely used to describe the adsorption from diluted solution but yields no maximum value of adsorption at saturation.

Sips model takes account three parameters from Freundlich and Langmuir models, and assumes that each adsorption site interacts with a single molecule or ion of the adsorbate surface Eq. (11.5):

$$q_e = \frac{q_m \left(K_s C_e\right)^{1/n}}{1 + \left(K_s C_e\right)^{1/n}} \tag{11.5}$$

Where K_s is sips binding constant ($L\ mg^{-1}$)^n, and n is the heterogeneity factor; n close to or equal to 1 takes place in biosorbents with homogeneous active sites whereas a value close to 0 takes places in biosorbents with heterogeneous active sites. The n_s parameter obtained with the Ni(II) and Cr(III) adsorption data in simple systems was 0.51 and 0.65 respectively, these values between 0 and 1 describe the degree of homogeneity/heterogeneity of the adsorption sites due a greater concentration of superficial groups with the same capacity of adsorption in terms of energy according Guarín-Romero et al. (2019).

BET (Brunauer, Emmett and Teller) isotherm equilibrium model is a multilayer model, and it assumes that a Langmuir isotherm applies to each layer and that there is equal energy of adsorption for each layer except for the first layer Eq. (11.6):

$$q_e = \frac{q_s C_{BET} C_e}{\left(C_s - C_e\right)\left[1 + \left(C_{BET} - 1\right)\left(\frac{C_e}{C_f}\right)\right]} \tag{11.6}$$

Where q_s is the theorical saturation capacity using the Langmuir isotherm (mg g^{-1}), C_{BET} the BET constant which indicates energy of surface interaction ($L.mg^{-1}$). In Table 11.2, the main results of different types of natural agro-industrial wastes and by-products for heavy metal removal are summarized.

In most cases, Langmuir isotherms were able to simulate the experimental data better than Sips and Freundlich models with a high correlation coefficient and is often used to determine the maximum sorption capacity of biosorbent.

The majority of authors consider the low sorption capacity of byproducts and agro-industrial waste to be a main problem for their application but is necessary to note that those sorbents work most effectively in treatment of very dilute solutions, enabling very low concentration of pollutants to be achieved.

Table 11.2 Adsorption isotherms models data obtained on biosorption of different ion metals and other pollutants on agro-waste biosorption

Biosorbent	Pollutant	Operation conditions			Results			References
		pH	T (°C)	C_0 (mg. L^{-1})	q_{exp} (m. g^{-1})	Isotherm model	q_{cal} (m.g^{-1})	
Banana peels	Cd (II) Pb (II)	3 5	25	0.05		Langmuir	q_m: 2.18 5.71	Anwar et al. (2010)
Soybean meal	Cr (III) Cu(II)	5	20	100	15.6 14	Sips	q_m: 23.5 39.6	Witek-krowiak (2013)
Olive oil	Cr (VI)	2	60	200	16.49	Langmuir	q_m:18.69	Malkoc (2006)
Aloe vera waste	U(VI) Cd(II)	4 5			201.2 70.4			Noli et al. (2019)
Pretreated orange peel	Cr(III) Fe(III)	3		10 30		Langmuir	q_m: 9.43 18.19	Lugo-Lugo et al. (2012)
Corncobs	Sulfamethoxazole	6	20	20	0.56	BET	q_s: 0.50	Peñafiel et al. (2019a)
Grape pomance	Aflatoxin B1 Zearalenone Ochratoxin A Fumonisin B	7	37	1 1 2 2	4.9 1.12 0.64 0.12	Sips Langmuir Freundlich Langmuir	q_m: 4.7 2.7 2.5 1.6	Avantaggiato et al. (2013)

Kinetics Study

The adsorption rate between sorbate and biosorbent in equilibrium is evaluated with kinetic models and rate limiting steps. The pseudo-first and pseudo-second order are the most widely used kinetic models to evaluate the biosorption of heavy metals and emerging compounds on agro-waste.

Pseudo-first order. Adsorption process occurs through first-order chemical reactions, where the rate constant is independent of concentration Eq. (11.7):

$$\frac{dq_t}{dt} = k_1\left(q_e - q_t\right) \tag{11.7}$$

Where k_1 is rate constant of pseudo-first order model (min^{-1}) and q_t is amount adsorbed at time t ($mg.g^{-1}$). Generally, the calculated q_e differs significantly of experimental q_e although high correlation coefficient is obtained.

Pseudo-second order. Also considered a chemical reaction but second order. Involving valence forces through sharing or exchange of electrons between biomass and metal ions Eq. (11.8):

$$\frac{dq_t}{dt} = k_2\left(q_e - q_t\right)^2 \tag{11.8}$$

Where k_2 is rate constant of pseudo-second order model ($g.mg^{-1}.min^{-1}$).

Intraparticle diffusion model presented by Weber and Morris is a model derived from Fick's second law of diffusion Eq. (11.9):

$$q_t = k_p t^{1/2} + C \tag{11.9}$$

Where K_p is the intraparticle diffusion rate constant ($mg.g^{-1}.min^{-1/2}$) and C is a constant for any experiment (mg/g) and has been reported by several researchers to involve two forms, the first one to get a straight line that passes through the origin when adsorption capacity at any time (q_t) plotted against the square root of time ($t^{1/2}$), and the second one, when two or three steps are involved in the whole process, in the plot q_t versus $t^{1/2}$, has multilinearity, the first step considers an external instantaneous surface adsorption, the second step is controlled by intraparticle diffusion therefore is a gradual adsorption, and the third step is the final equilibrium step (Wu et al. 2009). Wu et al. plotted the curves with various initial adsorption factors (R_i) and considered four zones of the initial adsorption according to R_i value; from 0 to 1 were classified, zone 1 for weakly initial adsorption, zone 2 for intermediately initial adsorption, zone 3 for strongly initial adsorption and zone 4 pro completely initial adsorption. For example, the kinetics for phenol compounds on active carbons belonged to zone 3. Therefore, the shape of adsorption isotherm is so important and is associated with the formation of monomolecular or multimolecular layer adsorption via both strong and weak adsorbate–adsorbent interactions (Abdolali et al. 2014)

Continuous Systems

Most research using biosorbents for metal ions are based on batch kinetic and batch equilibrium studies. However, in the practical operation of full-scale sorption processes, continuous-flow fixed-bed columns are often chosen. In such systems, the concentration profiles in the liquid and sorbent phases change in both space and time. From the perspective of process modelling, the dynamic behaviour of a fixed-bed column is described in terms of the effluent concentration–time profile, that is, the breakthrough curve. As a result, the development and application of predictive and simulative mathematical models for the design of continuous biosorption processes represent an important area in environmental engineering. The determination of model parameters and the verification of model validity can be obtained by well-designed, laboratory-scale experiments. With potentially enormous environmental applications in detoxification of metal-bearing industrial effluents, biosorption processes are considered as not only technically feasible but also economically very attractive.

Mathematical Backgrounds

From a practical point of view, biosorption processes to great scales are carried out in a continuous way (Park et al. 2010). In these systems, the concentration in the liquid phase and in the solid phase varies both in space and in time, due to which, the design and optimization of fixed-bed columns is especially difficult if not approached through a quantitative model. In this sense, the dynamic behaviour of fixed-bed columns is described in terms of 'exit concentration–time', that is to say, what is known as breakthrough. A typical breakthrough curve represents the relationship of the entry concentrations to the exit concentrations in time or the circulated volume. When the fluid passes through the column, an area of mass-transfer is defined that varies from 0% of the initial concentration (corresponding to the sorbent without solute) to 100% of the initial concentration (corresponding to the total saturation).

The point where the metal concentration in the effluent reaches a certain value, generally related with the permitted limit for that metal by regulations and environmental norms, is called the breakthrough point, and corresponds to the breakthrough time (t_b) that allows determining the volume of treated effluent. From a practical point of view, the saturation time (t_s) is set when the metal concentration in the effluent has a value between 90% and 95% of the initial concentration of that metal in solution.

To describe the breakthrough curve, numerous models have been proposed that can be from semi-empiric simple models of a few parameters that exist and easy to solve mathematically, to rigorous models that consider axial dispersion in the flow direction, resistance to the film diffusion, diffusion intra matter, which can include

diffusion in the surface and in the pores that generally require complicated numeric solutions (Chu 2003). These models are not only used to analyse and interpret experimental data, they also are used to predict the response of the systems when the operation conditions are changed (Joo et al. 2010). The performance of packed-bed column is described according to the concept of the breakthrough curve that is the plot of time versus effluent concentration:

Effluent volume is calculated from Eq. (11.10):

$$V_{\text{eff}} = Qt_{\text{t}} \tag{11.10}$$

where t_{t} represents the total time (min) and Q is the flow that circulates through the column (mL. min^{-1}).

The area under the breakthrough curve obtained by integrating the adsorbed concentration versus time plot can be used to find the total adsorbed metal quantity. Total adsorbed metal quantity in the column (q_{t}) for a given feed concentration and flow rate is calculated from Eq. (11.11):

$$q_{\text{t}} = \frac{Q}{1000} \int_{t=t_{\text{t}}}^{t=0} C_{\text{R}}\, dt \tag{11.11}$$

where C_{R} is the concentration of retained metal (mg.L^{-1}).

Total amount of metal sent to column is calculated from Eq. (11.12):

$$m_{\text{t}} = \frac{C_0 Q t_{\text{t}}}{1000} \tag{11.12}$$

Total removal percent of metal (column performance) with respect to flow volume can also be calculated from the ratio of total quantity of metal adsorbed to the total amount of metal passed through the column from Eq. (11.13):

$$\text{Removal } (\%) = \frac{q_{\text{total}}}{m_{\text{total}}} \tag{11.13}$$

The breakthrough curve, typically S-shaped, represents a valuable tool for evaluating the biosorbent efficiency. Indeed, the amount of solute removed at saturation can be easily evaluated by calculating the area above the breakthrough curve, whose slope provides information about the column service time. The main features of the breakthrough curve are the breakthrough and saturation/exhaustion points which theoretically correspond to an abrupt rise (infection point) in the effluent concentration plot and the complete column saturation, respectively. The time elapsed until attaining the breakthrough point directly affects the service time of the column. In laboratory experiments, packed bed columns are usually operated until the saturation point is attained. Conversely, in industrial applications, the column is usually regenerated when the effluent metal concentration exceeds a breakthrough/service point, which is prefixed depending on the metal toxicity. When the breakthrough point is attained, the effluent concentration can slowly rise to the saturation point

(flattened breakthrough curve). However, it is preferable to have a steep slope which corresponds to a shorter mass transfer zone (Vijayaraghavan and Yun 2008). The shape of the breakthrough curve is affected by many parameters, such as flow rate, inlet metal concentration, pH, bed height and bed particle size (Kumar et al. 2016).

Most of the models for continuous sorption systems have been developed to predict the breakthrough curves. Some examples are reported in Table 11.3. The Adams–Bohart model is usually applied to the initial part of the breakthrough curve and is obtained by combining two kinetic equations, the first describing the solute

Table 11.3 Column adsorption models (Patel 2018; Ahmed and Hameed 2018; Acheampong et al. 2013; Vijayaraghavan and Prabu 2006)

Breakthrough curve model	Equation	Remarks	Nomenclature
Thomas model	$\frac{C_0}{C} = 1 + \exp\left(\frac{k_{TH}}{F}\left(Q_0 M - C_0 V_{eff}\right)\right)$	One of the most widely used methods to describe column biosorption, which assumes Langmuir kinetic of sorption–desorption and second-order reversible reaction kinetic	k_{TH} is the Thomas model rate constant ($mg^{-1}\ g^{-1}$), Q_0 is the maximum solid-phase concentration of the solute (mg g^{-1}), V_{eff} is the volume of metal solution (L)
Adams–Bohart	$\frac{C}{C_0} = \exp\left(k_{AB} C_0 - k_{AB} N_0 Z / v\right)$	Rate of adsorption depends upon concentration of the sorbing species and residual capacity of adsorption	k_{AB} is the kinetic parameter ($L.mg^{-1}.min^{-1}$) N_0 is the saturation concentration (mg. L^{-1}), Z is the bed length (cm) and v is the superficial velocity ($cm.min^{-1}$)
Yoon–Nelson model	$\frac{C}{C_0} = \frac{\exp\left(k_{YN} t - \tau k_{YN}\right)}{1 + \exp\left(k_{YN} t - \tau k_{YN}\right)}$	Assumes that the rate of decrease in the probability of adsorption for each sorbate molecule is proportional to the probability of sorbate sorption and the probability of sorbate breakthrough on the sorbent	k_{YN} is the Yoon–Nelson model rate constant (min^{-1}), τ is the time required for 50% adsorbate breakthrough (min)
Modified dose–response model	$\frac{C}{C_0} = 1 - \frac{1}{\left(V_{eff} / b_{MDR}\right)^{a_{MDR}}}$		a_{MDR} and b_{MDR} are the modified dose–response model constants

(continued)

Table 11.3 (continued)

Breakthrough curve model	Equation	Remarks	Nomenclature
Bed depth service time (BDST)	$t = \frac{N_0}{C_0 v} Z - \frac{1}{k_{BDST} C_0} \ln\left(\frac{C_0}{C_t} - 1\right)$	Based on the Bohart and Adams quasi-chemical rate law, the rate of the sorption process is directly proportional to the fraction of sorption capacity still remaining on the media. This model is provided by the relationship between bed depth and service time	k_{BDST} is the rate constant ($L.mg^{-1}.h^{-1}$), v is the linear velocity ($cm.h^{-1}$)
Clark model	$\frac{C}{C_0} = \left(\frac{a}{\left(1 + A_c e^{-rt}\right)}\right)^{\frac{1}{n-1}}$	Column adsorption is mass-transfer concept with combination of Freundlich isotherm and behaviour of flow in column is of piston type.	n is the Freundlich parameter and A and r are the Clark Constants. The introduction of parameter a to take into account that the curve is not perfectly symmetrical at the point $C = 0.5C_0$

transfer from the liquid phase, the second governing the sorption accumulation on the biosorbent A similar equation has been obtained by Wolborska (1989), who also takes the solute axial diffusion into account. The Thomas model has been used in the linear form to quantify the maximum adsorption capacity of the adsorbent bed. In the Clark model, the breakthrough curve is obtained by adopting the Freundlich equation. The model introduced by Yoon and Nelson (1984) is much simpler as it does not require specific information about the adsorbate/adsorbent system.

Vera et al. (2019) investigated the use of lead(II) and cadmium(II) biosorption with sugarcane bagasse and cocoa shell in fixed-bed columns. The hydrodynamic study was performed by varying the diameter and height of the column, as well as the diameter and mass of the biosorbent, to determine the best hydrodynamic conditions, which resulted in a flow through the column of 2.12 $mL.min^{-1}$. The experimental data were adjusted to several models that describe the rupture curve for one and two component systems.

As we see in Fig. 11.2a, b, for single-component systems the area under the curve is greater for Cd^{+2} than for Pb^{+2}, deducing that the greater absorption corresponds to Pb^{+2}, which it is due to a greater affinity to the bagasse active sites for Pb^{+2} more than Cd^{+2}. Table 11.4 shows the parameters obtained from the analysis of the experimental data presented in the rupture curves, for single-components and two-components with the sugar cane bagasse.

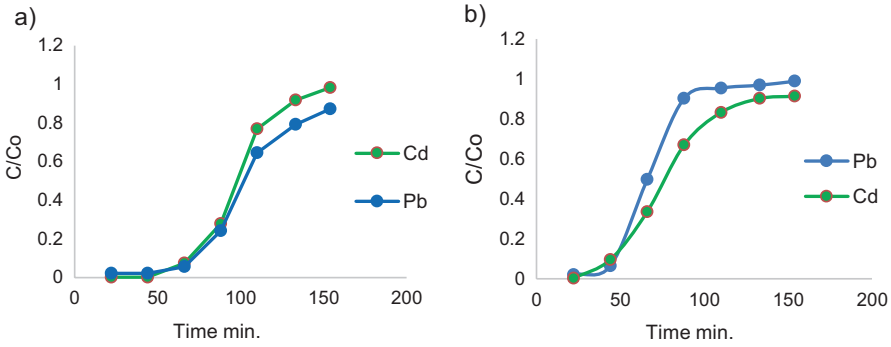

Fig. 11.2 (**a**) Rupture curve for adsorption of Pb^{+2} and Cd^{+2}, in a column of fixed bed filled with sugar cane bagasse in single-component system. (**b**) Rupture curve for adsorption of Pb^{+2} and Cd^{+2} in a column of fixed bed filled with sugar cane bagasse in two-component system

Table 11.4 Rupture curves parameters for adsorption of Pb^{+2} and Cd^{+2} in columns of fixed bed using sugar cane bagasse

		Single-component system		Two-component system	
Parameters		Pb(II)	Cd(II)	Pb(II)	Cd(II)
Rupture curves	tr (min)	74	70	47	43
	ts (min)	168	128	88	129
	Vr (mL)	118.4	112	76.61	70.09
	q_b (mg.g^{-1})	0.154	0.146	0.1	0.091
	SNU (cm)	15.67	5.14	13.05	18.67
	M_{total} (mg)	2.29	2.29	2.33	2.33
	q_t (mg)	2.08	2.07	2.08	2.16
	% adsorption	91	90	89.3	92

According to data obtained by the rupture curves, in the single-component and two-component system, the amount of metal that passes through the column (Mtotal) and the maximum adsorption capacity (q_t), they are equivalent to Pb^{+2} and Cd^{+2}. In the single-component system, the parameters which varied in lead and cadmium, they are the times of rupture and saturation (tr y ts), the volume treated at rupture point (Vr), the adsorption capacity (q_b), the not used fixed lying (SNU), being reported higher values for Pb^{+2} than for Cd^{+2}.

Regarding removal, the bagasse showed an adsorption percentage, practically equal for lead and cadmium. However, in the two-component system, data shows that lead and cadmium interaction in solution caused a significant decrease in all values of the variant parameters from single component systems, though some parameters were superior for cadmium and others for lead, as in case of rupture time, in lead (47 min) it was slightly superior than cadmium (43 min), so the volume treated for lead (76.6 mL) is superior than cadmium (70.09 mL), moreover for saturation time, the higher value registered was for cadmium, (129 min) compared to

lead (88 min), that means after the rupture, the competition of the active sites by metals of concern, favoured Cd^{+2}, this one which had the highest affinity for lead. The adsorption capacity proved to be equal for both metals, at the no used fixed bed, cadmium reported the highest value with 18.63 cm. About removal, the bagasse showed a higher adsorption percentage for cadmium with a removal of 92% instead of lead which showed 89%. In conclusion, in the single-component system, lead has greater affinity to sugar cane bagasse active sites than cadmium, however, when these two metals are in interaction, there is a greater affinity by cadmium, the affinity order being Cd > Pb.

As shown in the Fig. 11.2a, Dose–Response model is the best-adjusted model to the rupture curve of experimental adsorption of Pb^{+2}, with a R^2 factor correlation of 0.97. The Thomas model is the least adjusted to rupture curve, though its R^2 is more than 0.9. The Yoon–Nelson model adjusts acceptably to experimental data with a R^2 equal to 0.99; however the values of the time required to retain 50% of initial metal, τ, they are very similar to those obtained experimentally in sugar cane bagasse, which coincides with the findings of several researchers studying different biosorbent–metal systems in fixed bed column. For the adsorption of cadmium (Fig. 11.2b), the Yoon–Nelson model is the best curve that fits to the experimental data with a R^2 registered of 0.99; the values of τ, experimentally and calculated by the model are equal. The Dose–Response model has an allowable adjustment with cadmium experimental rupture curve, with a R^2 of 0.9. The least adjusted model is Thomas', though its R^2 is equal to 0.97 the generated curve, underestimates the experimental values.

For two-component system, Yoon–Nelson, Thomas, and Dose–Response models were separately applied, in order to appreciate the adjustments of rupture curves modelled with experiments. Figure 11.3a compares experimental rupture curves of lead and cadmium with those adjustment curves obtained from the Yoon–Nelson model. The Yoon–Nelson model does not adjust properly to experimental rupture

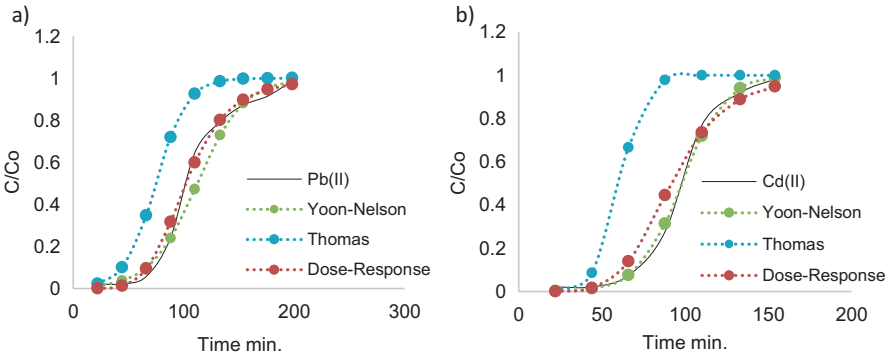

Fig. 11.3 (**a**) Comparison between Pb^{+2} experimental rupture curves and those obtained by applied models based on time in column filled with sugar cane bagasse. (**b**) Comparison of the experimental rupture curves of Cd^{+2} with those obtained by applied models based on time in column filled with sugar cane bagasse

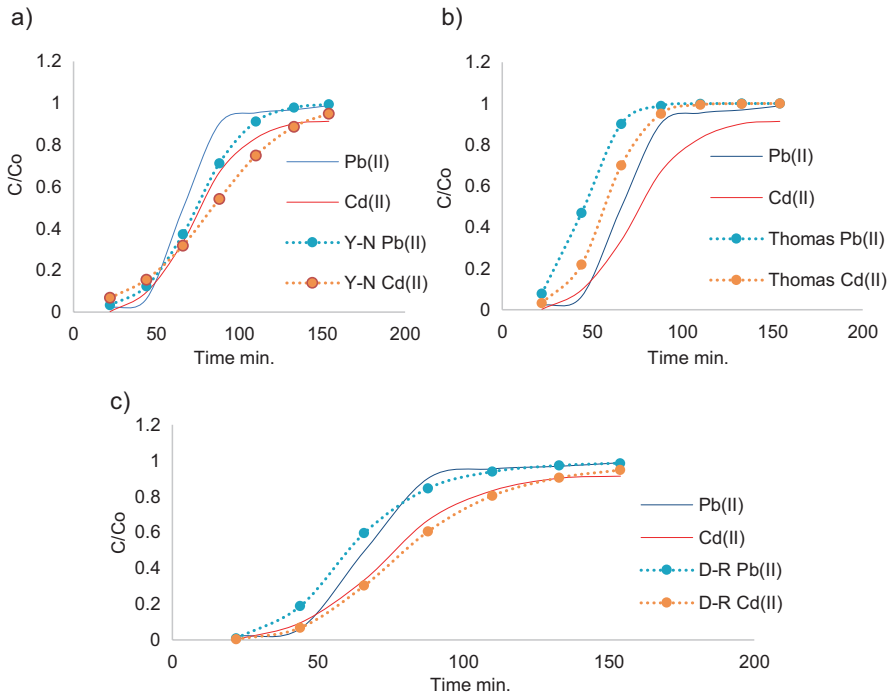

Fig. 11.4 (**a**) Comparison of the experimental rupture curves of Pb^{+2} y Cd^{+2} with those obtained by Yoon–Nelson model in column filled with sugar cane bagasse in T–C system. (**b**) Comparison of the experimental rupture curves of Pb^{+2} y Cd^{+2} with those obtained by Thomas in column filled with sugar cane bagasse in T–C system. (**c**) Comparison of the experimental rupture curves of Pb^{+2} y Cd^{+2} with those obtained by Dose–Response model in column filled with sugar cane bagasse in T–C system

curves of lead and cadmium in a two-component system; the modelled curves with Yoon–Nelson showed a R^2 of 0.94 for lead and 0.93 for cadmium. Figure 11.3b compares the experimental rupture curves of lead and cadmium with those adjusted curves obtained from Thomas model (based on time). The curves obtained by the Thomas model does not adjust to any studied metals (Fig. 11.4).

From all models based on time, the Dose–Response model is the best adjusted to experimental data for both lead and cadmium. With R^2 values equal to 0.96 for lead and 0.99 for cadmium. Regarding the adsorption capacities, the experimentally obtained values for sugar cane bagasse in a two-component system, corresponds to 0.1 $mg.g^{-1}$ for lead and 0.09 $mg.g^{-1}$ for cadmium, similar values were obtained from Thomas model, 0.094 $mg.g^{-1}$ for lead and 0.11 $mg.g^{-1}$ for cadmium. Using the parameters found with this model, it is possible to obtain an expression that reproduces the columns behaviour in other experimental conditions, with no need for further experiments. The biosorption of Pb^{+2} and Cd^{+2} with cocoa shell in fixed bed was also investigated. The experimental data were fitted to several models describing the breakdown curve for single component and two component systems. The

removal percentages of lead and cadmium in single-component systems are 91% and 90%, respectively. In bicomponent systems with Pb–Cd the percentage of lead removal was 88% and cadmium was 90%. The Dose–Response model in two-component and single-component systems was the one that best reproduced the experimental rupture curves throughout the measured range (Vera et al. 2018).

Rodriguez (2015) investigated the removal Cr^{6+} and Ni^{2+} by sugarcane bagasse in two up-flow fixed-bed columns in series have been presented. The experimental data were adjusted for several kinetic models that described the breakthrough curve obtained for a single column and for two columns in series. The Dose–Response model is the one that better adjusts the experimental data for the studied metals with a high correlation coefficient.

Perspectives

Over the last years, biosorption has received considerable attention from academic researchers, becoming one of the most promising and cost-effective alternative technologies for heavy metal removal and recovery from industrial wastewaters. However, despite the high number of scientific studies on biosorption, several technical and scientific aspects still need to be clarified for the commercialization and the spread of this technology at industrial scales. Based on these considerations, future research may be focused on the characterization and identification of new materials to be used as biosorbents with higher cost-effectiveness and biosorption efficiency, enhancement of selective metal biorecovery through biosorption in multi-metal systems, and development of analytical tools based on deterministic mathematical models able to describe multi-sorbate systems.

References

Abbas, S., Ismail, I., Mostafa, T., & Sulaymon, A. (2014). Biosorption of heavy metals: A review. *Journal of Chemical Science and Technology, 3*(4), 74–102.

Abdolali, A., Guo, W., Ngo, H., Chen, S., Nguyen, N., & Tung, K. (2014). Typical lignocellulosic wastes and by-products for biosorption process in water and wastewater treatment: A critical review. *Bioresource Technology, 160*, 57–66.

Acheampong, M., Rakshirajan, K., Annachhatre, A., & Lens, P. (2013). Removal of Cu(II) by biosorption onto coconut shell in fixed-deb column systems. *Journal of Industrial and Engineering Chemistry, 19*, 841–848.

Ahalya, N., Ramachandra, T., & Kanamadi, R. (2003). Biosorption of heavy metals. *Research Journal of Chemistry and Environment, 7*, 71–79.

Ahmed, M., & Hameed, B. (2018). Removal of emerging pharmaceutical contaminants by adsorption in fixed-bed column: A review. *Ecotoxicology and Environmental Safety, 149*, 257–266.

Ali, S., Athar, M., Salman M., & Din, M. (2011). Simultaneous removal of Pb(II), Cd(II) and Cu(II) from aqueous solutions by adsorption on Triticum aestivum - a green approach. *Hydrology Current Research 2*, 118.

Ali, I., Asim, M., & Khan, T. (2012). Low cost adsorbents for the removal of organic pollutants from wastewater. *Journal of Environmental Management, 113*, 170–183.

Al-Mohammedawi, H., Znad, H., & Eroglu, E. (2019). Improvement of photofermentative biohydrogen production using pre-treated brewery wastewater with banana peels waste. *International Journal of Hydrogen Energy, 44*(5), 2560–2568.

Alomá, I., Rodríguez, I., Calero, M., & Blázquez, G. (2013). Biosorption of Cr6+ from aqueous solution by sugarcane bagasse. *Desalination and Water Treatment, 52*, 31–33.

Anwar, J., Shafique, U., Zaman, W., Salman, M., Dar, A., & Anwar, S. (2010). Removal of Pb(II) and Cd(II) from water by adsorption on peels of banana. *Bioresource Technology, 101*, 1752–1755.

Avantaggiato, G., Greco, D., Damascelli, A., Solfrizzo, M., & Visconti, A. (2013). Assessment of multi-mycotoxin adsorption efficacy of grape pomace. *Journal of Agricultural and Food Chemistry, 62*, 497–507.

Basha, S., Murthy, A., & Jha, B. (2008). Sorption of Hg(II) from aqueous solutions onto Carica papaya: Application of isotherms. *Industrial and Engineering Chemistry Research, 47*(3), 980–986.

Bhatt, R., Kushwaha, S., Bojja, S., & Padmaja, P. (2018). Chitosan-thiobarbituric acid: A superadsorbent for mercury. *ACS Omega, 3*(10), 13183–13194.

Bilal, M., Rasheed, T., Sosa-Hernández, J. E., Raza, A., Nabeel, F., & Iqbal, H. M. N. (2018). Biosorption: An Interplay between Marine Algae and Potentially Toxic Elements—A Review. *Marine Drugs, 16*(2), 65.

Boudrahem, F., Soualah, A., & Aissani-Benissad, F. (2011). Pb(II) and Cd(II) removal from aqueous solutions using activated carbon developed from coffee residue activated with phosphoric acid and zinc chloride. *Journal of Chemical & Engineering Data, 56*(5), 1946–1955.

Chabannes, M., Garcia-Diaz, E., Clerc, L., Bénézet, J. C., & Becquart, F. (Eds.). (2018). Lime and hemp or rice husk concretes for the building envelope: Applications and general properties. In *Lime hemp and rice husk-based concretes for building envelopes* (Springer briefs in molecular science) (pp. 1–101). Cham: Springer..

Chao, H., Chang, C., & Nieva, A. (2014). Biosorption of heavy metals on citrus maxima peel, passion fruit shell, and sugarcane bagasse in a fixed-bed column. *Journal of Industrial and Engineering Chemistry, 20*(5), 3408–3414.

Chowdhury, S., & Saha, P. D. (2011). Biosorption kinetics, thermodynamics and isosteric heat of sorption of Cu(II) onto Tamarindus indica seed powder. *Colloids and Surfaces B: Biointerfaces, 88*(2), 697–705.

Chu, K. (2003). Prediction of two-metal biosorption equilibria using a neural network. *The European Journal of Mineral Processing and Environmental Protection, 3*, 119–127.

De Oliveira, A., Rizzato, T., Barros, B., Favaro, S., Caetano, W., Hioka, N., & Batistela, V. (2019). Physicochemical modifications of sugarcane and cassava agro-industrial wastes for applications as biosorbentes. *Bioresource Technology Reports, 7*, 100294.

Deng, X., & Wang, P. (2012). Isolation of marine bacteria highly resistant to mercury and their bioaccumulation process. *Bioresource Technology, 121*, 342–347.

Dinesh, M., & Kunwar, P. (2002). Single- and multi-component adsorption of cadmium and zinc using activated carbon derived from bagasse from agricultural waste. *Water Research, 36*(9), 2304–2318.

Fernández-González, R., Martín-Lara, M.-A., Iáñez-Rodríguez, I., & Calero, M. (2018). Removal of heavy metals from acid mining effluents by hydrolyzed olive cake. *Bioresource Technology, 268*(July), 169–175.

Gadd, G. M. (2008). Biosorption: Critical review of scientific rationale, environmental importance and significance for pollution treatment. *Journal of Chemical Technology and Biotechnology, 84*, 13–28.

Gadd, G. M., & White, C. (1985). Copper uptake by Penicillium ochro-chloron: Influence of pH on toxicity and demonstration of energy dependent copper influx using protoplasts. *Journal of General Microbiology, 131*, 1875–1879.

Gaur, N., Kukreja, A., Yadav, M., & Tiwari, A. (2018). Adsorptive removal of lead and arsenic from aqueous solution using soya bean as a novel biosorbent: Equilibrium isotherm and thermal stability studies. *Applied Water Science, 8*(4), 1–12.

Gh, A., Sohrab, K., & Ghorbanian, A. (2018). Experimental and modeling investigation of thorium biosorption by orange peel in a continuous fixed-bed column. *Journal of Radioanalytical and Nuclear Chemistry, 317*(2), 871–879.

Gilbert, U. A., Emmanuel, I. U., Adebanjo, A. A., & Olalere, G. A. (2011). Biosorptive removal of Pb2+ and Cd2+ onto novel biosorbent: Defatted Carica papaya seeds. *Biomass and Bioenergy, 35*(7), 2517–2525.

Goyal, N., Jain, S. C., & Banerjee, U. C. (2003). Comparative studies on the microbial adsorption of heavy metals. *Advances in Environmental Research, 7*, 311–319.

Greene, B., & Darnall, D. W. (1990). Microbial oxygenic photoautotrophs (cyanobacteria and algae) for metal-ion binding. In H. L. Ehrlich & C. L. Brierley (Eds.), *Microbial mineral recovery* (pp. 227–302). New York: McGraw-Hill.

Guarín-Romero, J., Rodriguez-Estupiñán, P., Giraldo, L., & Moreno-Piraján, J. (2019). Simple and competitive adsorption study of nickel (II) and chromium (III) on the surface of the brown algae *Durvillaea antarctica* biomass. *ACS Omega, 4*, 18147–18158.

Hammaini, A., González, F., Ballester, A., Blázquez, M. L., & Muñoz, J. A. (2003). Simultaneous uptake of metals by activated sludge. *Minerals Engineering, 16*(8), 723–729.

Hamza, F., El-Aassy, I., & Guibal, E. (2019). Integrated treatment of tailing material for the selective recovery of uranium, rare earth elements and heavy metals. *Minerals Engineering, 133*(May 2018), 138–148.

Joo, J., Hassan, S., & Oh, S. (2010). Comparative study of biosorption of Zn^{2+} by *Pseudomonas aeruginosa* and *Bacillus cereus*. *International Biodeterioration & Biodegradation, 64*(8), 734–741.

Kahraman, S., Dogan, N., & Erdemoglu, S. (2008). Use of various agricultural wastes for the removal of heavy metal ions. *International Journal of Environment and Pollution, 34*(1/2/3/4), 275–284.

Khan, T., Singh, V., & Ali, I. (2009). Sorption of Cd(II), Pb(II), and Cr(VI) metal ions from wastewater using bottom fly ash as a low-cost sorbent. *Journal of Environmental Protection Science, 3*, 124–132.

Kumar, D., Pandey, L. K., & Gaur, J. P. (2016). Metal sorption by algal biomass: From batch to continuous system. *Algal Research, 18*, 95–109.

Lugo-Lugo, V., Barrera-Díaz, C., Ureña-Núñez, F., Bilyeu, B., & Linares-Hernández, I. (2012). Biosorption of Cr(III) and Fe(III) in single and binary systems onto pretreated orange peel. *Journal of Environmental Management, 112*, 120–127.

Malkoc. E., Nuhoglu, Y., Dundar, M. (2006). Adsorption of chromium(VI) on pomace—An olive oil industry waste: Batch and column studies. *Journal of Hazardous Materials, 318*(1), 142–151.

Memić, Š., Abdić, M., Šabanović, E., & Sulejmanović, J. (2018). Adsorptive removal of eight heavy metals from aqueous solution by unmodified and modified agricultural waste: Tangerine peel. *International journal of Environmental Science and Technology, 15*(12), 2511–2518.

Modak, J. M., & Natarajan, K. A. (1995). Biosorption of metals using nonliving biomass-a review. *Minerals and Metallurgical Processing, 12*, 189–196.

Moubarik, A., & Grimi, N. (2015). Valorization of olive stone and sugar cane bagasse byproducts as biosorbents for the removal of cadmium from aqueous solution. *Food Research International, 73*, 169–175.

Muhamad, H., Doan, H., & Lohi, A. (2010). Batch and continuous fixed-bed column biosorption of Cd2+ and Cu2+. *Chemical Engineering Journal, 158*, 369–377.

Nahar, K., Chowdhury, A., Chowdhury, A., Rahman, A., & Mohiuddin, K. (2018). Heavy metals in handloom-dyeing effluents and their biosorption by agricultural byproducts. *Environmental Science and Pollution Research, 25*, 7954–7967.

Nikiforova, T., & Kozlov, v. (2016). Regularities of the effects of the nature of polysaccharide materials on distribution of heavy metal ions in a heterophase biosorbent-water solution system. *Protection of Metals and Physical Chemistry of Surfaces, 52*, 399–424.

Noli, F., Kapashi, E., & Kapnisti, M. (2019). Biosorption of uranium and cadmium using sorbents based on Aloe vera wastes. *Journal of Environmental Chemical Engineering, 7*(2), 102985.

Norton, L., Baskaran, K., & McKenzie, T. (2004). Biosorption of zinc from aqueous solutions using biosolids. *Advances in Environmental Research, 8*(3–4), 629–635.

Nuhoglu, Y., & Malkoc, E. (2005). Investigations of nickel (II) removal from aqueous solutions using tea factory waste. *Journal of Hazardous Materials, 127*, 120–128.

Pagnanelli, F., Toro, L., & Veglio, F. (2002). Olive mill solid residues as heavy metal sorbent material: A preliminary study. *Waste Management, 22*, 901–907.

Panda, G., Das, S., Bandopadhyay, T., & Guha, A. (2007). Adsorption of nickel on husk of Lathyrus sativus: Behavior and binding mechanism. *Colloids and Surfaces B: Biointerfaces, 57*, 135–142.

Park, D., Yun, Y., & Moon Park, J. (2010). The past, present and the future trends of biosorption. *Biotechnology and Bioprocess Engineering, 15*, 86–102.

Patel, H. (2018). Fixed-bed column adsorption study: A comprehensive review. *Applied Water Science, 9*, 45.

Peñafiel, M., Matesanz, J., Vanegas, E., Bermejo, D., & Ormad, M. (2019a). Corncobs as a potentially low-cost biosorbent for sulfamethoxazole removal from aqueous solution. *Separation Science and Technology*, 1–13. https://doi.org/10.1080/01496395.2019.1673414.

Peñafiel, M., Vanegas, E., Bermejo, D., Matesanz, J., & Ormad, M. (2019b). Organic residues as adsorbent for the removal of ciprofloxacin from aqueous solution. *Hyperfine Interactions, 240*, 71.

Rocha, G., Nascimento, V., Gonçalves, A., Fernandes, V., & Martín, C. (2015). Influence of mixed sugarcane bagasse samples evaluated by elemental and physical-chemical composition. *Industrial Crops and Products, 64*, 52–58.

Rodriguez, I., Kumar, N., & Aloma, I. (2015). Modeling of two up-flow fixed-bed columns in series for the biosorption of Cr^{6+} and Ni^{2+} by sugarcane bagasse. *Desalination and Water Treatment, 53*(3), 792–805. https://doi.org/10.1080/19443994.2014.940395.

Schneider, I., Rubio, J., & Smith, R. (2001). Biosorption of metals onto plant biomass: Exchange adsorption or surface precipitation? *International Journal of Mineral Processing, 62*, 111–120.

Sreelatha, G., Kushwaha, S., Rao, V., & Padmaja, P. (2010). Kinetics and equilibrium studies of adsorption of anionic dyes using acid-treated palm shell. *Industrial & Engineering Chemistry Research, 49*(17), 8106–8113.

Sud, D., Mahajan, G., & Kaur, M. (2008). Agricultural waste material as potential adsorbent for sequestering heavy metal ions from aqueous solution – A review. *Bioresource Technology, 99*, 6016–6027.

Tsamba, A., Yang, J., Blasiak, W., & Wójtowicz, M. (2007). Cashew nut shells pyrolysis: Individual gas evolution rates and yields. *Energy and Fuels, 21*(4), 2357–2362.

Vera, L., Uguña, R., & Flores, M. (2016). Eliminación de los metales pesados de las aguas residuales mineras utilizando el bagazo de caña como biosorbente. *Afinidad, 573*, 43–49.

Vera, L., Uguña, R., & Flores, M. (2018). Biosorción de Cd (II) y Pb (II) en columna de lecho fijo con cáscara de cacao. *Afinidad, 75*(581), 16–22.

Vera, L., Uguña, R., & Flores, M. (2019). Fixed bed column modeling of lead(II) and cadmium(II) ions biosorption on sugarcane bagasse biosorption on sugarcane bagasse. *Environmental Engineering Research, 24*(1), 31–37.

Vijayaraghavan, K., & Prabu, D. (2006). Potential of *Sargassum wightii* biomass for copper(II) removal from aqueous solutions: Application of different mathematical model to bathc and continuous biosorption data. *Journal of Hazardous Materials, 137*, 558–564.

Vijayaraghavan, K., & Yun, Y.-S. (2008). Bacterial biosorbents and biosorption. *Biotechnology Advances, 26*, 266–291.

Volesky, B., & Schiewer, S. (2000). Biosorption, metals. In M. C. Flickinger & S. W. Drew (Eds.), *Encyclopedia of bioprocess technology: Processes fermentation biocatalysis and biosorption* (pp. 433–453). New York: Wiley.

Wang, J., Hu, N., Liu, M., Sun, J., & Xu, J. (2019). A novel core–shell structured biosorbent derived from chemi-mechanical pulp for heavy metal ion removal. *Cellulose, 6*, 8789–8799.

White, C., Sayer, J. A., & Gadd, G. M. (1997). Microbial solubilization and immobilization of toxic metals: Key biogeochemical processes for treatment of contamination. *FEMS Microbiology Reviews, 20*(3–7), 503–516.

Wiśniewska, M., & Nowicki, P. (2019). Simultaneous removal of lead(II) ions and poly(acrylic acid) macromolecules from liquid phase using of biocarbons obtained from corncob and peanut shell precursors. *Journal of Molecular Liquids, 296*, 111806.

Witek-Krowiak, A., & Reddy, D. H. K. (2013). Removal of microelemental Cr(III) and Cu(II) by using soybean meal waste – Unusual isotherms and insights of binding mechanism. *Bioresource Technology, 127*, 350–357

Wolborska, A. (1989). Adsorption on activated carbon of p-nitrophenol from aqueous solution. *Water Research 23*(1), 85–91.

Wu, F., Tseng, R., & Juang, R. (2009). Initial behavior of intraparticle diffusion model used in the description of adsorption kinetics. *Chemical Engineering Journal, 153*, 1–8.

Yoon, Y. H., & Nelson, J. H. (1984). Application of gas adsorption kinetics I. A theoretical model for respirator cartridge service life. *American Industrial Hygiene Association Journal, 45*(8), 509–516.

Zouboulis, A., Matis, K., & Hancock, I. (1997). Biosorption of metals from dilute aqueous solution. *Separation and Purification Methods, 26*, 255–295.